Masteroppgave

NTNU
Norges teknisk-naturvitenskapelige universitet
Fakultet for ingeniørvitenskap
Institutt for maskinteknikk og produksjon

Peder Loe Nystog

High Performance Engine Design And Optimization

Masteroppgave i Mechanical engineering
Veileder: Terje Rølvåg
Juni 2019

NTNU
Kunnskap for en bedre verden

Peder Loe Nystog

High Performance Engine Design And Optimization

Masteroppgave i Mechanical engineering
Veileder: Terje Rølvåg
Juni 2019

Norges teknisk-naturvitenskapelige universitet
Fakultet for ingeniørvitenskap
Institutt for maskinteknikk og produksjon

NTNU
Kunnskap for en bedre verden

Summary

In this master thesis performance upgrades of the CRF250L engine has been studied. Performance and durability are improved by increasing engine displacement to $305cm^3$ and upgrading internal engine components. The focus has been the crankshaft and the connected components, with the intent to optimize them for higher performance output. The suggested methods of improvement is based on previous and current race engine design, as well as on the possibilities within the CRF250L engine, gathered from research in the preliminary project paper.

The CRF250L engine has been built within the Fedem sofware, with the objective to analyze the crankshaft system. Original and new optimal engine components have been designed, and tested in the Fedem virtual test bench. Siemens NX linear and nonlinear analysis has been performed to investigate the possibility of catastrophic failure due to buckling. As suggested in the preliminary project paper, an H shaped titanium rod has proved beneficial, combining high strength and low weight.

Sammendrag

I denne master oppgaven er mulighetene for høy ytelses optimalisering av CRF250L motoren blitt studert. Ytelse og pålitelighet har blitt forbedret gjennom å øke motorvolum til $305cm^3$ og optimalisere interne komponenter. Fokuset har vært på veivakslingen og de tilhørende komponentene, med hensikt å optimalisere dem for økt ytelse. De foreslåtte metodene for å forbedre motoren er basert på tidligere og nåværende racing design, samt mulighetene tilstede i CRF250L motoren. Informasjonen er samlet i den foregående prosjektoppgaven.

CRF250L motoren har blitt bygget opp i Fedem programvaren, med hensikt å analysere veivaksling-systemet. Originale og optimaliserte motorkomponenter har blitt designet, og testet i testbenken i Fedem. Lineær og ikke-lineær analyse i Siemens NX har blitt gjennomført for avdekke muligheten for buckling i rådene. Som foreslått i den foregående prosjektoppgaven har det vist seg fordelaktig å benytte seg av et råde av titan med et H-formet tverrsnitt. Dette kombinerer høy styrke med lav vekt.

Preface

This master thesis is a continuation of the project paper the sharing same title. Large parts of chapter 2 and 3 originate from the preliminary paper. Following master thesis is to be submitted to the Norwegian University of Science and Technology (NTNU). The work has been carried under supervision of Terje Rølvåg at the Department of Mechanical and Industrial Engineering (MTP) in cooperation with MXRR.

Table of Contents

List of Figures

List of Tables

Abbreviations

TDC	=	Top Dead Center
BDC	=	Bottom Dead Center
RPM	=	Rotation Per Minute
CFD	=	Computational Fluid Dynamics
FE	=	Finite Element
MBS	=	Multi body Simulation
DOF	=	Degree of Freedom
KPI	=	Key Performance Indicator
CMS	=	Component Mode Synthesis
LC	=	Load Case
CAD	=	Computer Aided Design
OEM	=	Original Equipment Manufacturer

Chapter 1

Introduction

1.1 Background

The CRF250L motorcycle has been manufactured to fill a marked segment for people wanting an affordable dual-sport commuter motorcycle. Reviews from owners indicate the desire for more power. The possibility of increasing engine performance as well as maintaining durability is studied and recorded in this master thesis. Optimization through reverse engineering of the CRF250L engine, and utilizing both Siemens NX and Fedem software to design and analyze the structural integrity of the critical engine parts. In addition design and development of new components will be based on the study of previous and current racing technologies.

1.2 Objective

The objective is to uncover and analyze different possibilities of improving performance of the CRF250L engine, utilizing current race engine design to improve production OEM parts. Utilizing current race engine design developed on both analytic and empiric data. The main task is to implement a new engine to the virtual test-bench in Fedem to observe the key performance indicators, then suggest design alterations and realize them for the CRF250L application. In addition obtain quality data on the modifications made to the CRF250L engine, utilizing Siemens NX and Fedem software to achieve these objectives. Following tasks developed by the supervisor (Terje Rølvåg) were to be solved.

- Reverse engineer the stock HONDA CRF 250L engine.
- Design an optimal connecting rod type based on Falicon or MXRR CRF250R designs. Optimize the rod for the desired CRF250L performance.
- Select an optimal piston pin and bearing from MXRR for the wanted CRF250L performance.

- Identify load cases / KPIs (max compression and tension) in the FEDEM test bench to quantify the structural integrity of all critical engine components on the stock and optimized CRF250L engines.

Initially in cooperation with MXRR a new connecting rod design was tested. In this master thesis the results are taken into account and refined. While conducting a more extensive analysis of the critical parts.

Chapter 2

Theory

2.1 The Four Stroke Cycle

Due to the design of the four stroke engine, it operates in four different strokes, each stroke with a different purpose. The complete cycle can be represented as shown in figure 2.1. Following the Otto cycle presented in figure 2.2.

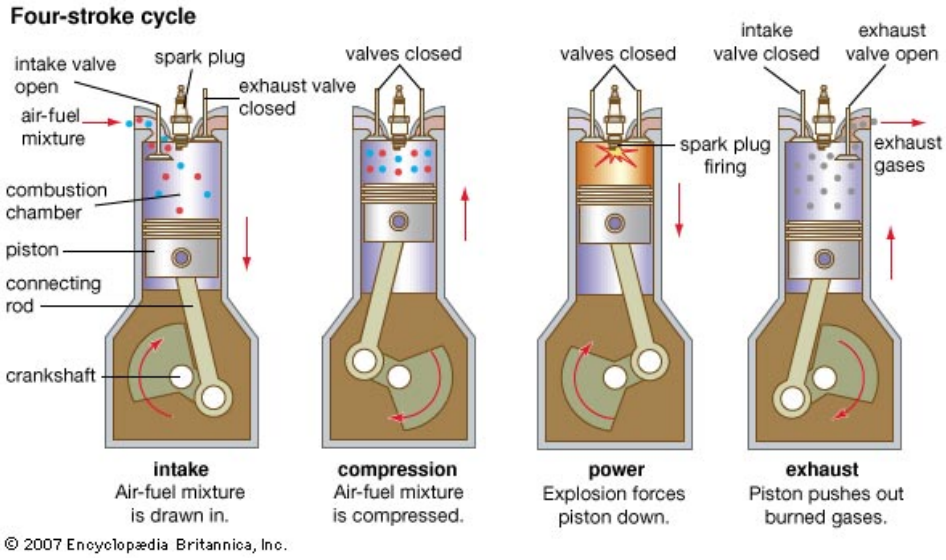

Figure 2.1: Four stroke engine cycle [Encyclopdia-Britannica-Inc (2018b)]

During the intake stroke, fuel and air is drawn into the cylinder through the intake valve, due to the low pressure generated by the downward piston movement. The amount of fuel and air mixture drawn into the cylinder is the basis for potential chemical energy

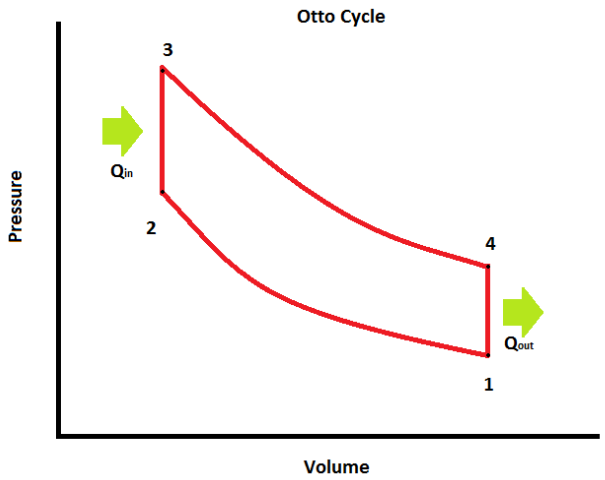

Figure 2.2: Otto cycle

to be converted into kinetic mechanical energy as shown in figure 2.2. When the piston passes bottom dead centre (BDC) the piston changes direction and the compression stroke begins. Both valves stay closed at this point to allow increase of pressure. The importance of compression can be viewed in figure 2.3 including the thermal efficiency equation. After reaching top dead center (TDC) the fuel and air mixture is ignited by the spark plug. The power stroke is the working stroke, driven by the expanding gasses from the combustion. This is the only stroke generating power. Again the piston reaches BDC. To expel the cylinder of the exhaust gases, the exhaust valves is opened as the piston moves upwards pumping the gases out of the cylinder.

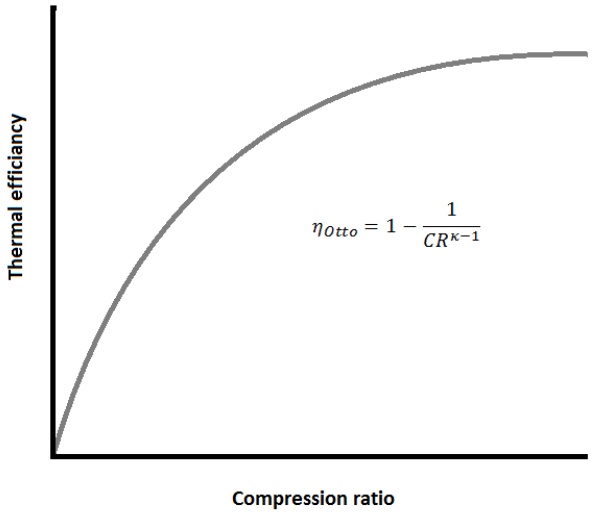

Figure 2.3: Efficiency Otto cycle

Utilizing a slider crank mechanism, the movement created in the cylinder is transferred into rotational movement, in such a way that the crankshaft is providing torque to the transmission.

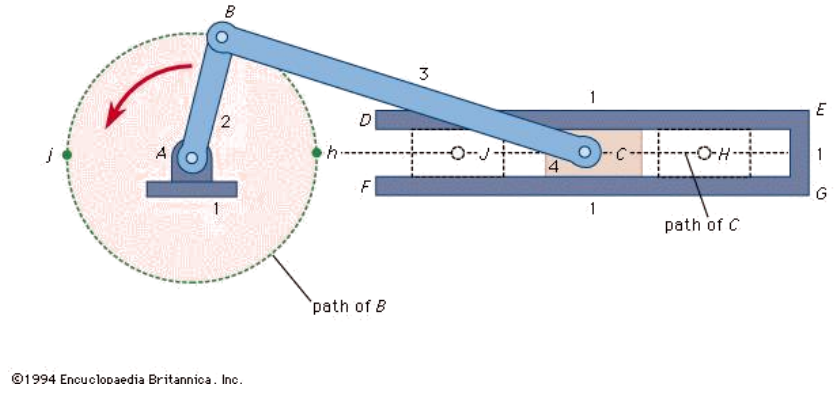

Figure 2.4: Four stroke engine cycle [Encyclopdia-Britannica-Inc (2018a)]

The slider crank mechanism is a simple way to explain the internal engine mechanism. The representation in figure 2.4 is beneficial when analyzing the main forces in play. Only

difference to the CRF250L engine is the offset crank in relation to the slider. An offset cylinder contributes to a more beneficial power stroke, as the piston is forced down closer to the tangent vector of the crank. The velocity vector of the piston is kept closer to the tangential direction of the rod/crank connection.

2.2 Parts to Consider

Crankshaft: It is powered by the combustion in the cylinder. Thermal and chemical power is converted to mechanical power. All other moving parts of an engine is driven by the crankshaft. When increasing the performance of an engine one need to consider all these parts as they can be subjected to higher loads.

Connecting rod and pin: The two common designs of connecting rods are I- and H-beam. Common materials used are steel, aluminum and titanium alloys. As with the crankshaft most of the same principles remain important. Reducing weight while maintaining structural integrity is a key performance factor. By reducing the weight of the rod, inertia forces and losses are reduced. Length of connecting rod and connecting point to the piston influence the lateral forces between piston and cylinder wall. Different ways of constructing the bearing in the big end of the rod is also an important factor. Either by using shell bearings with a split rod, or with a monolithic rod, one can reduce weight and improve crankshaft properties. Though uncommon in a single cylinder engine, where the crankshaft is pressed together. Generally done to accommodate a more durable roller bearing.

Timing Chain: Interlinking the crank- and camshaft. With a more powerful engine the acceleration may increase. Often with higher lifting cams and/or stiffer valve springs the force needed to rotate the cam is increased. Both instances increase the stress on the timing chain. As a result, crank and cam sprockets may also be subjected to increased wear.

Camshaft: The lobes is subjected to wear as they control the rockers. Cam lobe wear is reduced by sufficient lubrication, as tappets and rollers ride on the cam lobe. Aggressive grind and rocker ratio determine the contact pressure between tappet/roller and cam lobe, influencing wear.

Valves and springs: With a more aggressive cam lobe profile, higher revs and stiffer valve springs, the valves are subjected to higher forces. The valves must endure more tensile stress due to stiffer springs and more aggressive transitions from loading to unloading. The springs will need to be stiffer to accurately follow the cam profile as well as being able to compress more due to a higher lifting cam.

Bearings: Typically crank, transmission and cam bearings are the most affected. With high rotational speeds, roller bearings are applied. But in monolithic crankshaft design, split shell bearings has to be applied. Proper lubrication is key in such applications, in order to maintain sufficient lubrication film thickness. As with solid brass bearings, often used in the small end of the rod, where there are low rotational movement.

Clutch: With a higher revving and more powerful engine, the clutch is put under higher stress. When releasing the clutch, the friction between the clutch plates need to handle these elevated forces. Using more aggressive and durable discs in addition to stiffer clutch springs increases the grip by a higher friction coefficient and increased contact pressure.

Transmission: All gears from the crank all the way through the transmission to the end drive sprocket are subjected to higher forces as there are higher power output from the engine. Gear tooth width, transmission shaft diameters and bearings have to be able to handle the increase in power.

2.3 Specific Improvements to The CRF250L

2.3.1 The Crankshaft Assembly

In a performance crank shaft, weight is an influencing factor. Though the mass of a crankshaft will generate torque, excessive mass will also drain power due to the inertia of the rotating mass. In addition, more mass will lead to that the bearings and internal engine components are constantly affected by a more massive part, something that can lead to premature wear and fatigue. Tension in the connecting rod is a factor for failure, reducing the reciprocating masses will reduce the stresses caused by inertia loads. The reasons why the crankshaft still is the most massive moving part in an engine is as follows. Due to the stresses affecting a crankshaft during engine operation, some structural mass is required. As well as maintaining torque in the engine through the inertia of the rotating mass, additionally some mass is needed for crankshaft balancing. As the journal, connecting rod, wrist pin, piston etc. is a mass connected to only one side of the rotating crank (in a single cylinder engine) there has to be some mass to balance the contribution by these parts.

Balancing a crankshaft limiting the need for additional weight. This can be achieved by having the reciprocating components as light as possible and drilling the connecting rod journals, reducing weight in the heavy end of the crank. To the counterweight end of the crank, undercut flywheels are used in the CRF250L engine. That way the mass is places further from the center line of the crank, increasing the balancing effect with less material or mass.

Lubrication is another factor to consider. The big end of the rod is connected to the crank, with a bearing. With either a glider bearing or roller bearing sufficient oiling is important to reduce wear or catastrophic failure. One method is shaping the counterweights too increase oiling as well as reducing resistance through the oil in the sump. There is also the possibility to drill oil passages in the rod journals but will require a hollow journal, which is present in the current CRF250L engine. Cutting slots in the ends of the rod improve oiling as well.

2.3.2 Cylinder and Piston

Increasing engine displacement is a proven way to increase engine output. In the CRF250L engine there is a possibility to rebore the cylinder. As the cylinder has enough material to

be re-sleeved, increasing displacement to $305cm^3$, the possibility to repurpose the OEM cylinder is viable. A bigger and possibly higher compression piston has to be incorporated, the other parts of the engine has to be designed to manage the added weight of a larger piston.

2.3.3 Cylinder Head

Improving engine output by performing cylinder head port and polish is a proven performance upgrade. By reducing the surface roughness, the flow boundary layer is reduced, leading to better flow. To further enhance flow, material can be removed or added to create better flowing gates into and out of the combustion chamber. Drawbacks on this procedure is often lacking knowledge, method and high cost. Removing and adding material is a labour intensive job and is not automated, it is required to know exactly where to remove material and where to add. This has generally been obtained by trail and error process in the past, alternatively a computational flow dynamics (CFD) analysis could be performed. Manual work would still be required and can only replicate the simulation results accurately to some degree. Meanwhile the process of fluid porting is a interesting concept, as it yields better surface and flow properties. In addition the method is simple and less time consuming as it uses the original designed ports, and can be modified to fit many engines.

The throttle body of the current CRF250L is a 36 mm diameter unit. It might not be able to deliver the required amount of fuel to the updated system. The CBR250R and newer CRF250L has a 38mm unit, these are interchangeable parts make it easy and relatively cheap to accommodate the need for more fuel and air to the engine.

2.3.4 Valve Train

To further increase volumetric flow, higher lifting cams can be installed. Regrinds based on the design of the original cam is often used. Optimizing duration, phase and lift to a more race-oriented design. The CRF250R has higher lift and longer duration than the CRF250L. The more aggressive camshafts may require stiffer valve springs and/or stronger oversized valves. Accommodating oversized valves new seats must be ground and is generally a costly process.

Verifying that the springs can handle the increased loads, as well as that the springs themselves are stiff enough to follow the cam, as the valve springs experience higher accelerations and larger compression. Problems can occur when the cam is too aggressive for the springs as they will lose contact when valves are closing.

2.3.5 Rockers

A possible performance upgrade could be to install higher lift rockers. While maintaining the same parabolic signature of the camshaft lobes one will increase the lift and rate of lift. By maintaining the same camshaft, duration is unaltered. The cam will have the same basic characteristics. When introducing the higher ratio rockers, higher lift is possible. Increasing the volumetric efficiency. Gaining higher maximum lift, but also higher lift through the whole seat to seat duration. Allowing the engine to fill the cylinders with more air and fuel.

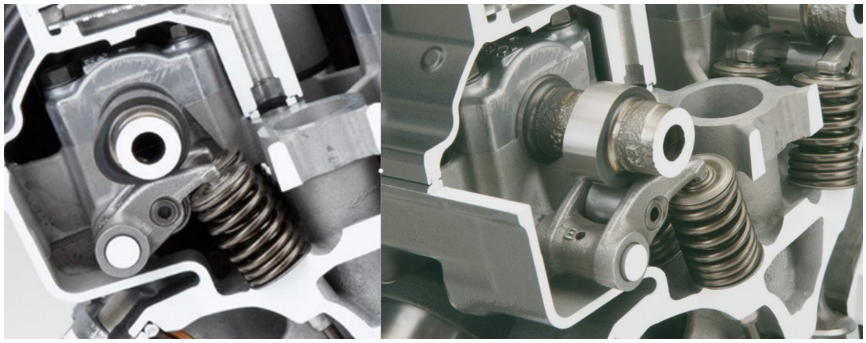

Figure 2.5: Current rocker setup Honda-Motor-Co. (2013)

By moving the roller closer to the rocker pivot shaft the ratio increases.As the roller move closer to the pivot shaft, a relief for the roller must be cut for clearance.

Higher stresses in the rocker arm will occur due to a longer lever. However, the design might show to be favorable as the roller shaft can be moved upwards, resulting in more material to handle to the loads. Moving the roller up higher might demand a smaller diameter roller to maintain correct clearance. By increasing the lever, the load on the cam and lobes is also increased.

2.4 Fedem

The Fedem-Technology-AS (2016) software has made the multi body simulation (MBS) presented in this paper possible, with the possibility to perform dynamic simulations. As dynamic analysis is more computational demanding than a static analysis, Fedem uses model reduction techniques to reduce computation and time consumption. Through CMS and super element technique model reduction is performed. The technique aim to reduce the number of DOFs, assuming only the lowest frequencies of vibration is the most important. The number of reduction or condensing methods apply the coordinate transformation on the form

$$\mathbf{v} = \mathbf{Hq} \tag{2.1}$$

Where $\mathbf{v}$ is the displacements in full form and $\mathbf{q}$ is the condensed set of displacements. Whereas $\mathbf{H}$ is a transformation matrix. The different ways of reducing the model result in a different construction of the transformation matrix. The dynamic condensing method used in Fedem combines modal reduction and static condensing.

Fedem has a result menu shown in figure 2.6, where the output is controlled by the user. Data must be specified preliminary to the simulation but can be loaded and viewed in its entirety after completion. Imported files in Fedem are reduced and simulated within the sofware. Fedem is a nonlinear solver, the high speed behaviour of the system presented in this paper require such a solver. Equilibrium equations through Newton Raphson iterations

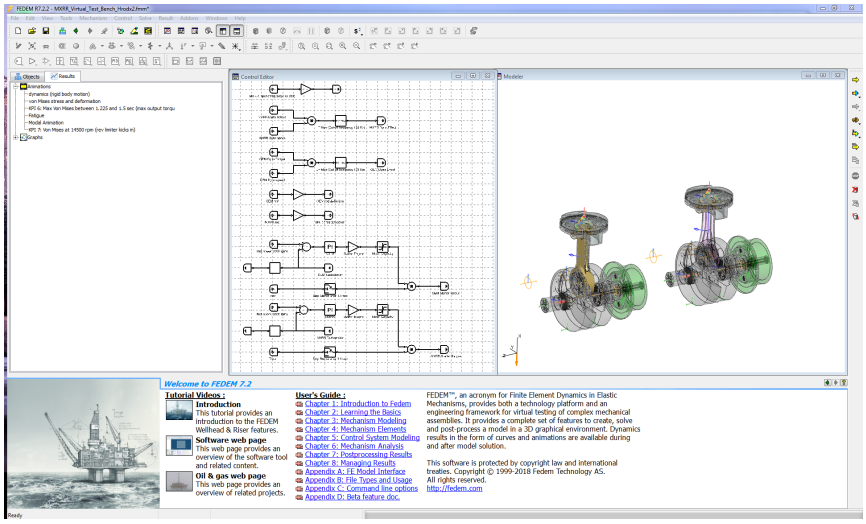

Figure 2.6: Fedem software

is used to correct the errors generated in the linear approximation around each increment starting point.

$$F_k^I + F_k + F_k^S = Q_k \tag{2.2}$$

In 2.2 the dynamic equilibrium of any time increment k. Where each term represent inertia forces, dampening forces and elastic forces sums up to the total input loads.

2.5 Siemens NX

The entire model is created in Siemens NX as individual parts. Mesh specific details can be viewed in chapter 4. The characteristics of the elements used are presented here. CTETRA10 is a four sided element with 10 nodes, used for solid body meshing with rather complex geometry. With such elements both Normal and shear stresses is an output option, given by the element grid points. When stress output is given there are several options. By looking at the difference between nodal average and elemental average one can evaluate the mesh. Nodal stresses tends to be higher as sharp corners produce stress concentrations, and nodal stresses might capture such a peak value. While an element will distribute all the nodal stresses. If the difference between nodal and elemental average is large it is an indicator that the mesh size is too large. There are two simple ways to solve this problem, by reducing element mesh size or idealizing geometry. R-type elements are used as placeholder elements. Being equal to a constraint equation utilizing several points. The RBE2 element is an example of such a rigid element. Producing a rigid connection through constraint equations between one single point to the arbitrary points, defining

the degrees of freedom. RBE elements might introduce false stiffness, and in that way influence results.

Chapter 3

Literature Study

3.1 Meng et al.(2005)

Effects of the connecting-rod-related design parameters on the piston dynamics and the skirt-liner lubrication by Meng et al. (2013), the authors study the effects of modifications to connecting-rod design. Monitoring some performance indicators as lateral forces against piston skirt, oil film thickness and frictional forces, while changing the design of the connecting-rod shown in figure 3.1. Changes done was among other length of rod, vertical and lateral piston pin offset, center of mass on connecting rod. Resulting from this research was a table of modifications and their influence on the performance indicators listed in the appendix. It was concluded that mass, length, rotational inertia and position of centre of mass was the factors contributing to largest differences in transverse forces. Piston pin offset and vertical placement had lower impact on transverse and side forces, but influenced oil film thickness and frictional force.

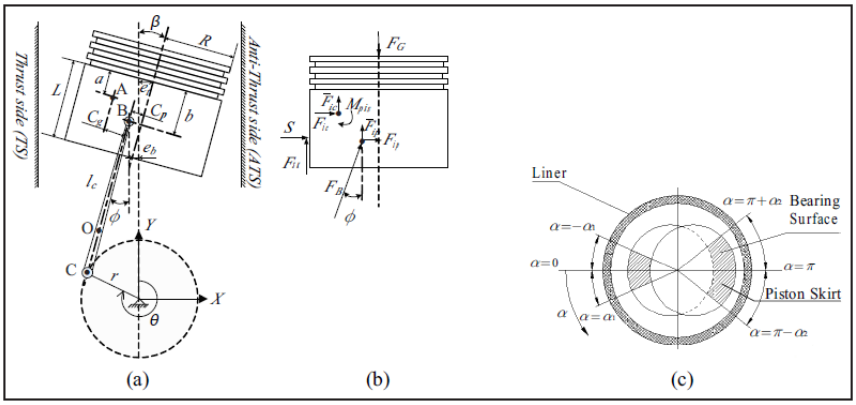

Figure 3.1: Meng et al. (2013) connecting rod critical regions

3.2 Hammil (2005)

The book Camshafts and Camshaft Tuning for High Performance Engines by Hammil (2005), explain the fundamentals of camshaft design and its characteristics. Understanding important terms as duration, lift, phase, overlap and valve clearance is fundamental. The internal combustion engine is not a new invention, there is massive amounts of knowledge available. Taking advantage of this knowledge is a time saving initiative. Most early and current knowledge about engines is gathered through trial and error. Basic guidelines is developed based on this knowledge. In Hammil (2005) camshafts are explained in rough terms, and certain guidelines is presented based on optimal performance versus reliability.

The most interesting part of the book is the chapter where the author present duration as the main differentiating factor of performance. As increased lift and rate of lift is generally always performance enhancing, duration changes the characteristic of the setup. With other words, duration has to be evaluated for each specific engine and its use. In the book a 270 cam is categorized as a typical mild cam, and a 300 degree cam as a racing cam. Both camshafts has the same general specifications only duration is changed. The two cams have completely different uses. Though duration also effect overlap, the time when both intake and exhaust valves are open at the same time, lift and phases is equal. Hammill emphasizes that the different duration cams all have their strengths and weaknesses. Designing the best camshaft for one specific engine will always be a trade off in some way. Longer duration will increase the engines top end power and ability to reach higher rpm, though low end power and torque suffers. Generally the two latter is aspects associated with everyday drivability in addition to the poor idle consistency caused by the increased overlap.

3.3 Strozzi et al. (2016)

A repertoire of failures in connecting rods for internal combustion engines, and indications on traditional and advanced design methods by Strozzi et al. (2016) is a paper on an in depth analysis on connecting rods. Initially introducing different ways a connecting rod can fail and the different design features. Drawing connections between design and failure modes, in relation to the critical areas of a connecting rod.

In figure 3.2 an overview of the different critical regions of connecting rod is presented. The area between small end and shank is prone to tension stresses caused by inertia forces, as well as compression from gas forces. Influence of small end stiffness and its relation to distributed forces in the piston pin. Strozzi et al. (2016) also takes a look at the big end, and the difference between the two main designs, monolithic and the split design. With a split big end there is more complicated interactions between parts and introduces different failure mechanisms. Interactions between parts is a recurring theme in the article. Movement of the bushing or even microslip can lead to lubrication failure or fretting fatigue respectively. Suggesting not only dimensions of the connecting rod, or severe force instances, is the sole reason for connecting rod failure.

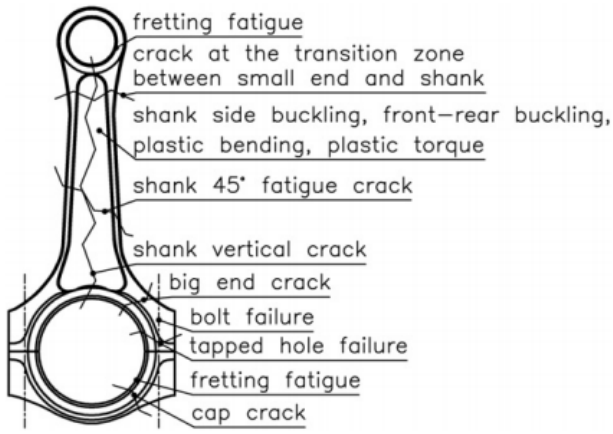

Figure 3.2: Strozzi et al. (2016) Connecting rod critical regions

3.4 Moon et al. (2007)

In the publication by Moon et al. (2007) the focus is on eliminating the error of the Merchant-Rankine equations for buckling. Given by:

$$Pcr = \frac{\pi^2 EI}{KL^2} \tag{3.1}$$

The challenges of integrating equation 3.1 is the irregular shape of the rod and its geometric gradient. Boundary conditions is another challenging area, as there is difficult to estimate the correct case when engine is in motion. In their finite element analysis the big end had a fixed constrained, the small end was allowed to move only in the loaded direction. Introducing quite strict conditions, as there are some amount of movement possible between parts, in addition to possible effects happening at high temperatures and rpm range. The conclusion from this paper was that the Merchant-Rankine equation did not apply to a shank of varying cross section. Further suggesting their own modified approach as a tool for suggesting a critical buckling load. In turn to be utilized for connecting rod development.

Chapter 4

Experiment

4.1 Reverse Engineering

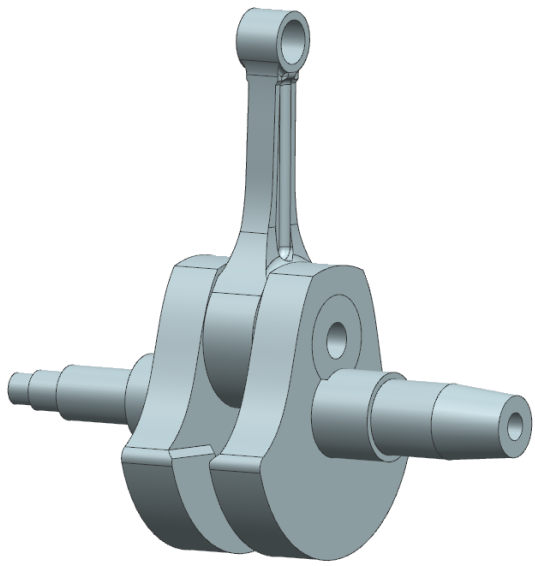

Figure 4.1: CRF250L Crank Assembly

Digital FEM's are required to generate the necessary .nas files supported by Fedem. To obtain correct and qualitative data, the stock CRF250L crankshaft had to be split and reverse engineered. By measuring dimensions of each component construction of a digital model (.prt files) is possible. The mass of all components were measured on a digital scale,

masses denoted in table 4.1. Having accurate mass ensures correct properties in the digital model. As well as comparing physical and digital mass is an indicator of the digital design accuracy. Parts have been idealized to allow a practical mesh. Features as small fillets, blends or holes with insignificant strength or stiffness contribution have been omitted. The assembled crankshft is presented in figure 4.1

Figure 4.2: OEM Connecting Rod

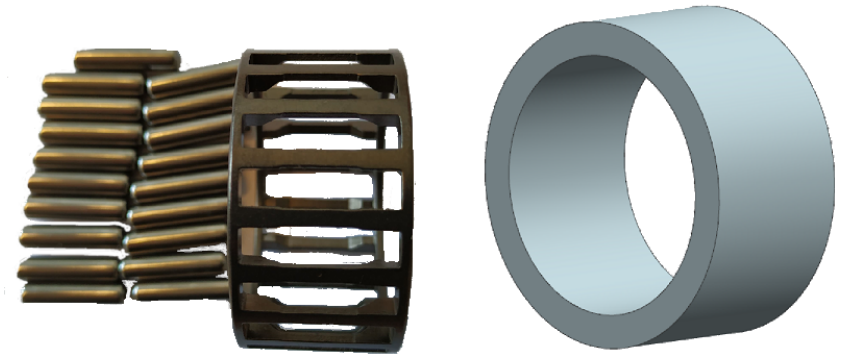

Figure 4.3: OEM Bearing

By using the spline function in Siemens NX to follow varying cross sections of the rod-

shank, an accurate digital representation was created. Chamfers and rounded edge were omitted in the CAD file as presented in figure 4.2 The bearing from figure 4.3 is modelled as a solid part with modified material properties to obtain correct mass contribution and stiffness. As the setup in Fedem takes care of losses due to contact, the bearing is no more than a placeholder for a connecting joint, its stiffness and mass.

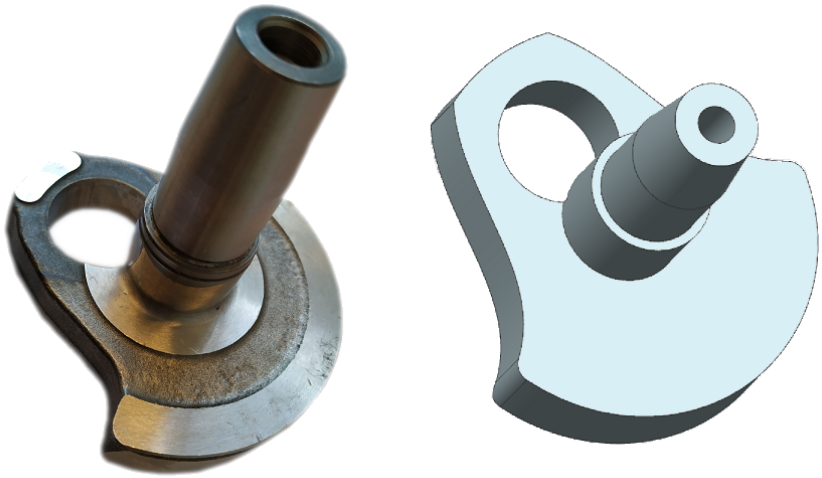

Figure 4.4: OEM Crankshaft Left

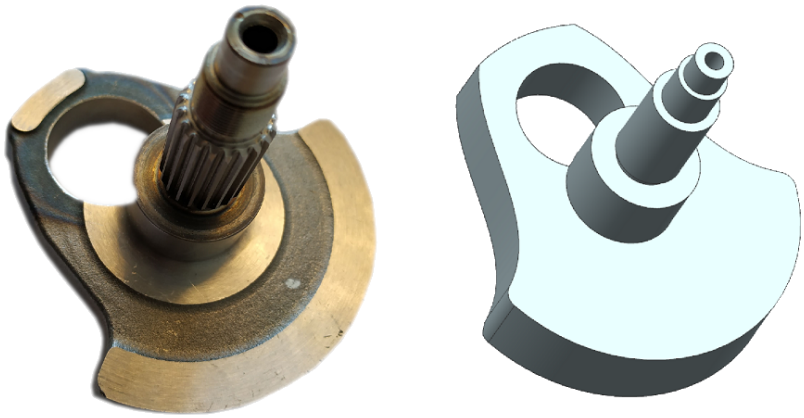

Figure 4.5: OEM Crankshaft Right

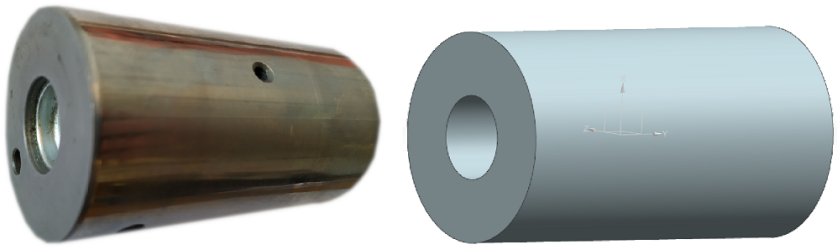

Figure 4.6: OEM Crank Pin

To easier match and assemble the two halves of the crankshaft in figure 4.4 and 4.5, the flywheel sketch with crank pin hole was basis for both sides. When assembling the crank pin in figure 4.6 the two sides of the crank and all connecting parts had a common reference. The largest idealization changes where done to the ends of the crank, including splines, threads and chamfers. Each far end of the crank is of less importance to the study, and can be severely idealized without compromising the results. The two shims are neglected from the model, their mass contribution is added to the two crank halves respectively.

Figure 4.7: OEM Crankshaft Shims

In table 4.1 the different component masses are displayed, obtained by measuring each component on a digital scale. The correct materials need to be assigned to each part and

Part:	Mass:
Connecting Rod	273.53 g
Bearing	64.10 g
Crank Pin	407.56 g
Crank Left	1456.50 g
Crank Right	1312.60 g
Shims 2pcs.	22.84 g

Table 4.1: Measured masses

a solid properties check can be run to evaluate the mass of the individual FEM files. The density of the crankshaft-steel had to be slightly lowered to obtain the corresponding mass. Deviations were small and the parts were measured on a precise scale. Deviations must come from CAD inaccuracies (idealization), or differences between library material and actual material. As it was a small deviation altering the density to match CAD and real life masses was chosen. Material can be viewed in appendix materials list.

4.2 Fedem Analysis Setup

The virtual test bench developed by Rølvåg and Bella (2017) has been is used to evaluate the both the original and the high output engines side by side. The dynamic test-bench is generated in the Fedem non linear dynamic software. Using the MBS software in addition to finite element analysis software the entire crankshaft mechanism can be considered. The general process is shown in figure 4.8.

The Fedem software require FE models, building a multi-body-system by interlinking FEM files, in this case from Siemens NX. Within the Fedem software, positioning and creating the correct interactions and boundary conditions, is possible. Using joints, springs and dampers. With the incorporated control system generator engine output and characteristics can be applied. By introducing the built in sensors like tachometers and strain rosettes it is possible to generate control parameters for the system as well as outputting the desired data. Similar to how represented by Rølvåg and Bella (2017) in figure 4.9.

Figure 4.9 display different parts of the Fedem model, but more importantly sensors, forces and joints. By testing with the exact same conditions the dynamic test bench is a viable tool for the purpose of engine optimization. Introducing identical parts, with the same properties and mesh, one can single out specific parts to review their influence on the system. The new engine has been rebuilt in Fedem. The OEM and high capacity engine is set up side by side.

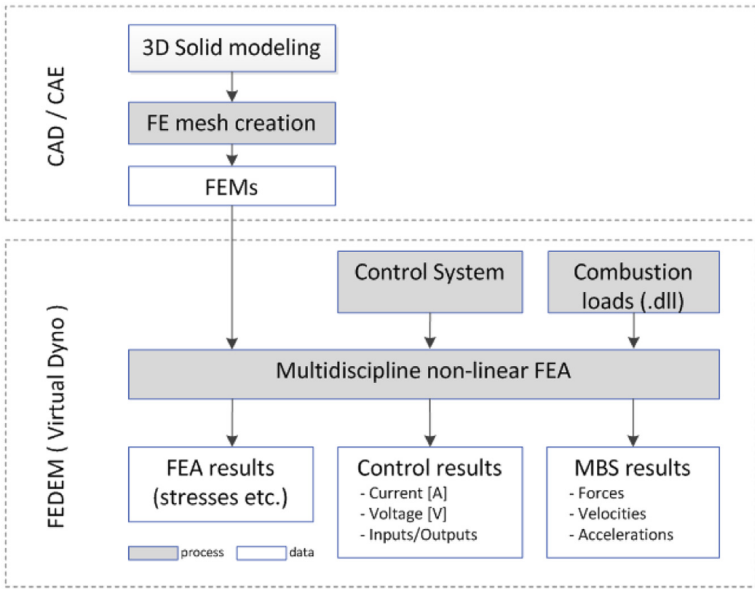

Figure 4.8: Rølvåg and Bella (2017) Fedem software method

The control system was created to observe some key performance indicators (KPI), to effectively and accurately provoke possible failures for the given application. The following incidents are specified in the simulation setup:

1. Electric starter is initiated, bringing the engine up to 3000 rpm, and engine fires.
2. Engine revs from 3000 under load.
3. Maximum compression plateau is reached.
4. Acceleration to maximum rpm, as a result of the dyno brake is turned off.
5. Brakes are turned back on with full throttle engaged.

The steps are designed to test different aspects of the engine. Initially testing the electric starter. Followed by a torque output benchmark as the engine is accelerated in the second step. In figure 4.10 the entire testing sequence is plotted. Keeping the engine at the calculated maximum compression range before increasing the rpm. By turning off the dyno brake the engine rpm increases, yielding ideal conditions for monitoring inertia forces. Suddenly turning the brake back on again reducing the rpm. Introducing a test for structural integrity by sudden increase in load, as if the clutch was released at max rpm from a standing still position. The Fedem test bench is set up to be an agile testing tool. To introduce other test designs, another FE model can be imported as a Nastran bulk data file and replace the existing one. This process is recorded in this paper. The CRF250L engine has been integrated in the test bench, and control system is regulated to output correct performance, shown in 4.11. Through component mode synthesis (CMS), Fedem performs model reduction, before initiating a new simulation.

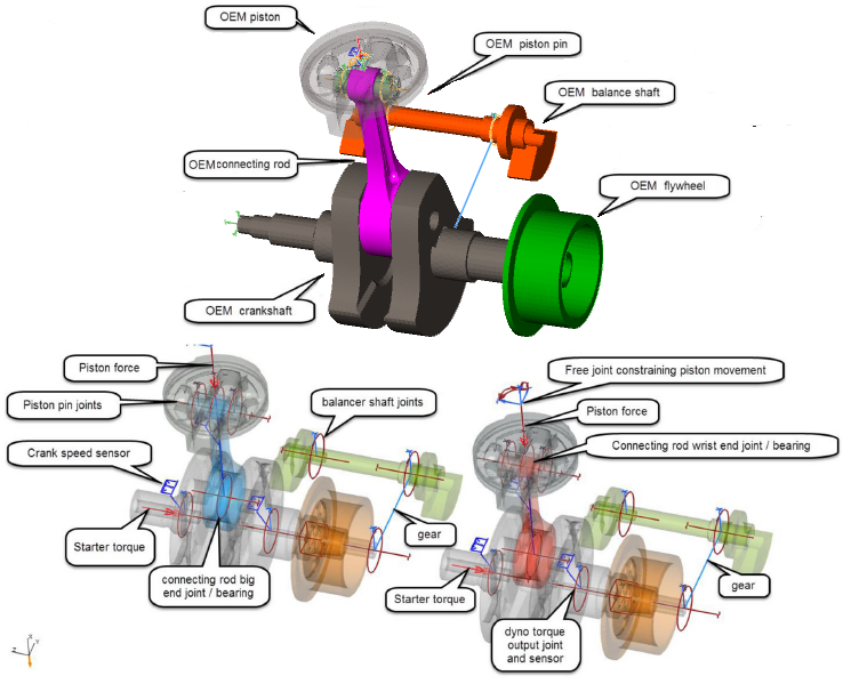

Figure 4.9: Rølvåg and Bella (2017) Modelled parts

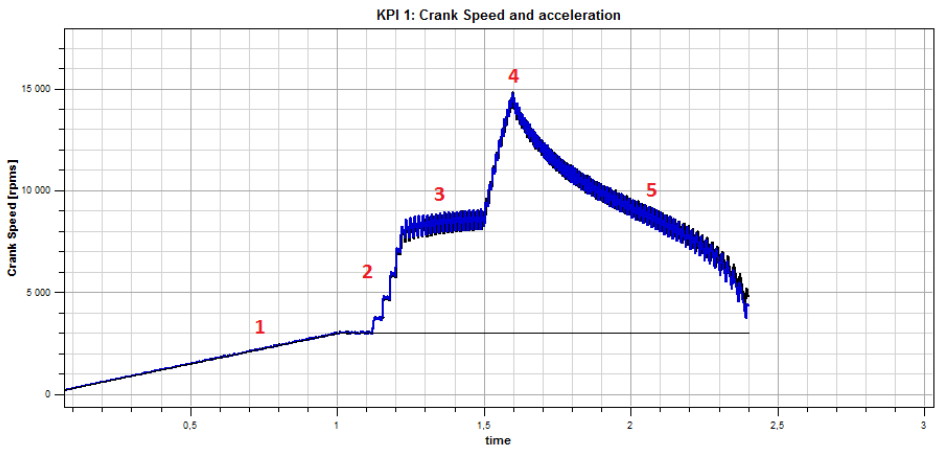

Figure 4.10: Testing sequence representation

Crank angle at max combustion pressure [360 degrees is TDC]	373.0
Standard deviation for combustion pressure [15-30 degrees]	17.0
Maximum gas pressure during combustion stroke [MPa]	10.5
Minimum pressure during suction stroke [MPa]	0.1
Maximum pressure during exhaust stroke [MPa]	0.6
Piston Area (set to 1 to get piston pressure) [mm^2]	1.0
Rev. limiter (no ignition above given rpm) [rpm]	14 500.0
Compression pressure (when no ignition) [MPa]	1.0

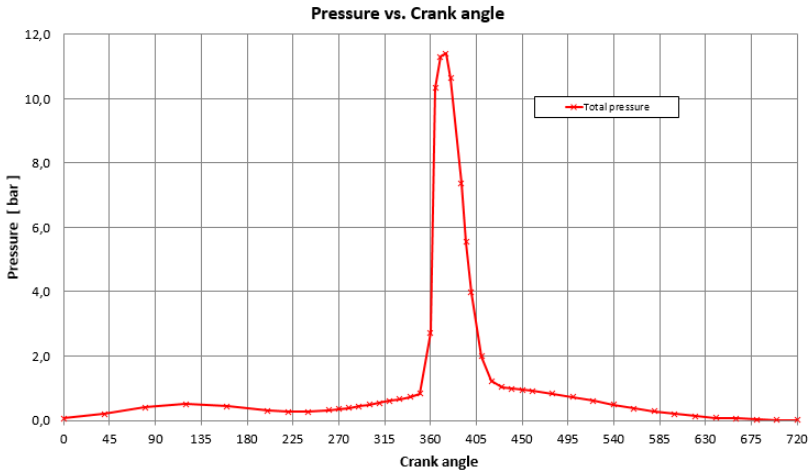

Figure 4.11: Modified pressure cycle for the CRF250L engine

4.2.1 Load Cases and Key Performance Indicators

Key performance indicators (KPIs) were established to benchmark the effectiveness of design modifications. Identifying load cases (LC) and testing for the different incidents is ideal to monitor possible problems with this specific engine application.

LC

- Maximum compression force in power stroke.
- Maximum tension stress at rpm limiter
- Performance alterations between systems

The load cases is related to real life incidents generated in the control system, shown in figure 4.10. Using he LC's, some measurable KPI's can be chosen. The aim is to optimize performance while maintaining reliability. The following KPI's will take both of these aspects into account.

KPI's

Of the output data from the analysis, the listed KPI's will be the main focus. Increasing performance and reducing stresses, loads and deflections would be beneficial.

- Performance increase
- Maximum axial deformation
- Maximum compression stresses
- Maximum tension stresses

4.3 Siemens NX Analysis Setup

The increase of power introduced by the big bore kit might lead to buckling of the OEM rod. As the rods are compressed with a significant load a small perturbation might provoke buckling. There are also several different ways such a perturbation may arise, load from skirt to piston contact is the most likely, but momentary lubrication failure might also be the cause. Results found by (Strozzi) clearly showed that buckling is a possible failure mode in connecting rods. While stress levels in a static or dynamic solver might be below yield, still buckling might occur. Performing a buckling analysis will unveil if the rods are susceptible to buckling.

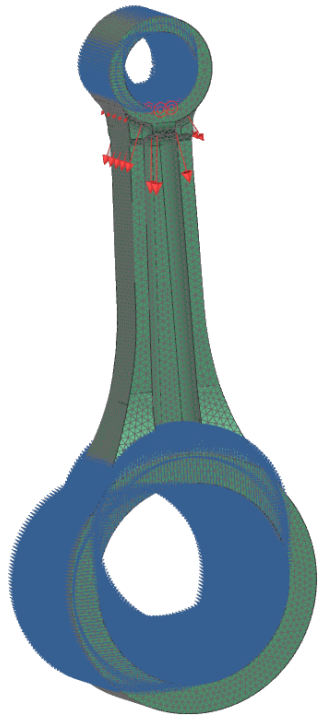

Figure 4.12: Buckling analysis loads and constraints

Investigating the possibility of buckling in the connecting rod is conducted in a combination of SOL105 and SOL106 in Siemens NX. By running a linear buckling analysis in SOL105 initially an approximate load level is obtained through the linear method, often called eigenvalue based buckling. Like a modal analysis the output of the analysis are several buckling modes. Unlike a modal analysis the first mode in buckling is the only interesting mode, as this is the first to occur at the lowest load level. Each buckling mode has a shape and value, the value represent the buckling load factor. This factor has to be multiplied with the applied load to obtain the suggested buckling load. In this case a load of 1 N was chosen, buckling mode will be one to one with buckling load. To obtain correct results the big end of the rod is fully constrained, apart from rotation about the crank pin, x-direction in this case. The small end was constrained to be free to move only in the load direction and free to rotate about the X-axis. The setup is shown in 4.12 and is similar to what was done by Moon et al. (2007). A bearing load of 1 N over 60 degrees of the small end was applied in compression as shown in figure 4.13 . By running a linear analysis the approximate buckling load is obtained in a short amount of time as the solver is time efficient.

Performing a nonlinear analysis with SOL106 a slightly higher load from SOL105 is used as a boundary load. The solver will add the load incrementally and continue until large

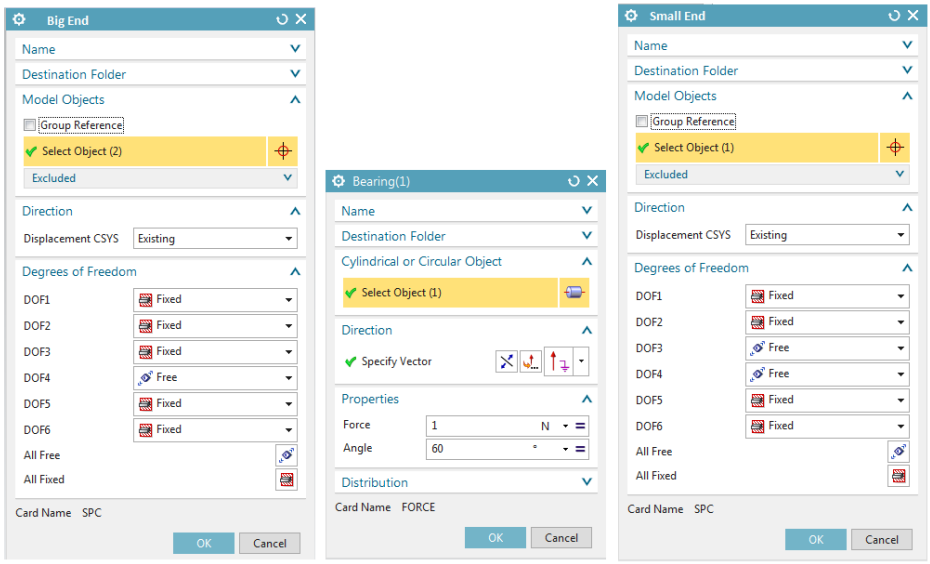

Figure 4.13: Load and Constraint specification

deformations occur, as the solver uses the load control approach. Several steps is necessary as the solver applies load incrementally to update the changes in structure stiffness. By introducing an eccentric load as well as the load from SOL105 a preliminary buckling load factor is suggested. Ranging from 0-1 a factor indicates the amount of load that was applied before large displacements occurred. Multiplying the total applied load with this factor gives a load to input in the nonlinear buckling analysis. The SOL106 buckling solver now has a a narrow nonlinear region to search for the correct buckling load. The result output is both stress distribution and buckling modes. Most interesting is the buckling factor, used to calculate the critical buckling load, given in 4.1.

$$P_{crit} = P_{applied} + (\alpha * \frac{P_{applied}}{NINC}) \tag{4.1}$$

The simulation was performed with 20 steps and updating the stiffness matrix every iteration. NINC in 4.1 refers to the amount of increments applied and α critical buckling factor.

4.4 Model

4.4.1 Piston

Comparison between the OEM and the high performance CRF250L start by constructing pistons to correct bore specification, as displacement is to be increased from $250cm^3$ to

$305cm^3$. Stock valve reliefs and piston pin size are maintained on both pistons. To accurately locate and position the piston force in Fedem a common surface had to be maintained, shown in 4.14. By utilizing synchronous modeling the outer faces of the OEM piston altered to 84mm.

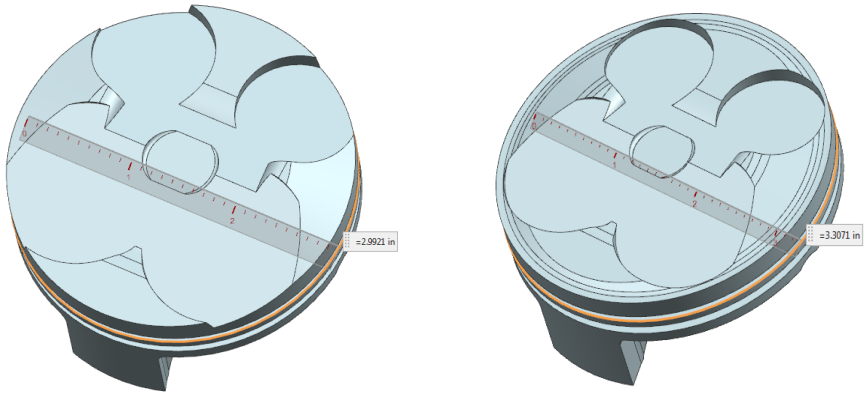

(a) OEM CRF250L Piston, diameter 76 mm **(b)** CRF250L Big Bore Piston, diameter 84 mm

Figure 4.14: Piston differences

4.4.2 Connecting Rod

In figure 4.15 three different connecting rods are modelled. The three different rods are possible design options, all with different capabilities. The Steel knife rod would later be deemed inferior to the titanium H-shaped rod. Therefore the OEM and H-shaped rod will be compared side by side in the Fedem test-bench.

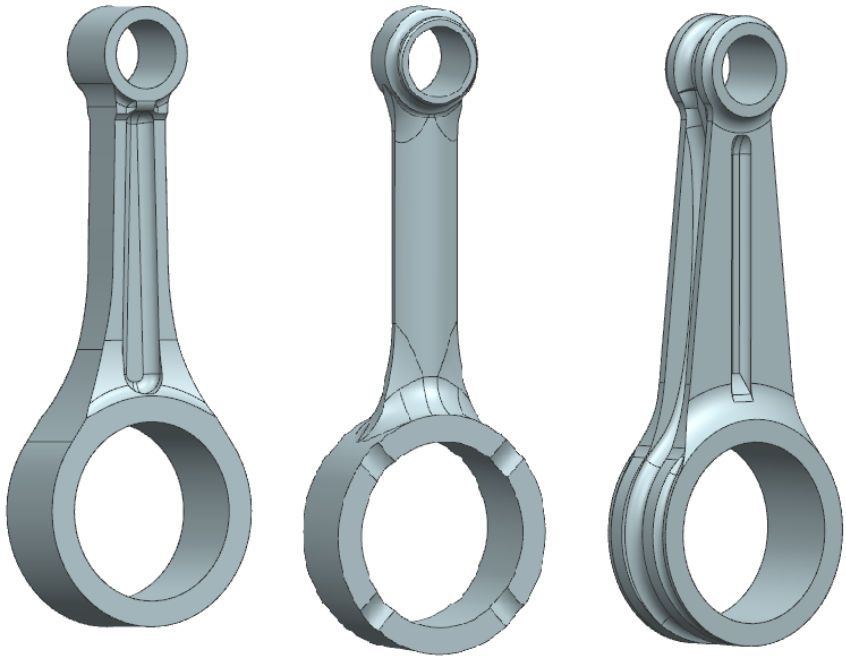

Figure 4.15: Oem steel rod, Steel Knife rod, Titanium H rod

Masses of each rod is measured and recorded in table 4.2. It is evident that there are large differences between the two materials, titanium being significantly lighter.

Connecting Rod Masses		
OEM Steel Rod	Steel Knife-Rod	Titanium H-Rod
273.5 g	262.4 g	161.6 g

Table 4.2: Differences in weight respective to figure 4.15

The specific H-shaped rod design shown in figure 4.15 is based on results gathered in the project paper which form the basis for this master thesis. The final chosen design is presented in 4.18. The conclusion leading to this design was found in the preliminary project paper, results from that paper follows.

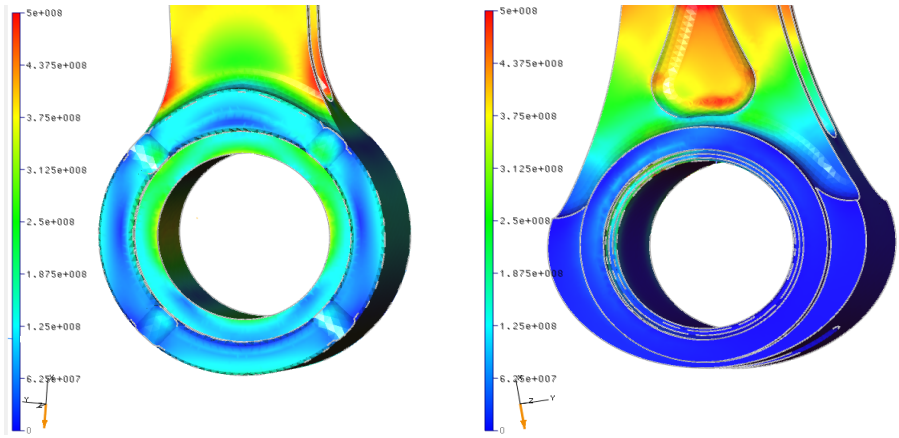

(a) Original MXRR rod **(b)** New oval MXRR rod

Figure 4.16: Oval design proved to reduce hoop stresses in the big end

By adding material to the lateral sides of the connecting rod big-end lead to reduced stress concentrations and smaller overall deflections, resulting in less wear on parts. Results can be seen in figures 4.16 and 4.17. The added material in the rod big end is to counter the stress concentrations and hoop stresses. In comparison to the OEM rod the total weight is reduced by more than 50%. In addition to improved strength the alterations seem to be influencing the performance in a positive way in some cases, there are less overall reciprocating mass, requiring smaller bob weights, meaning that the total mass is closer to the centre of the rotating axis of the crank. As a result, a more beneficial relationship between the rotating and reciprocating masses are obtained. The altered design based on the MXRR connecting rod is presented in figure 4.18, where the big end has been altered to accept a more durable roller bearing.

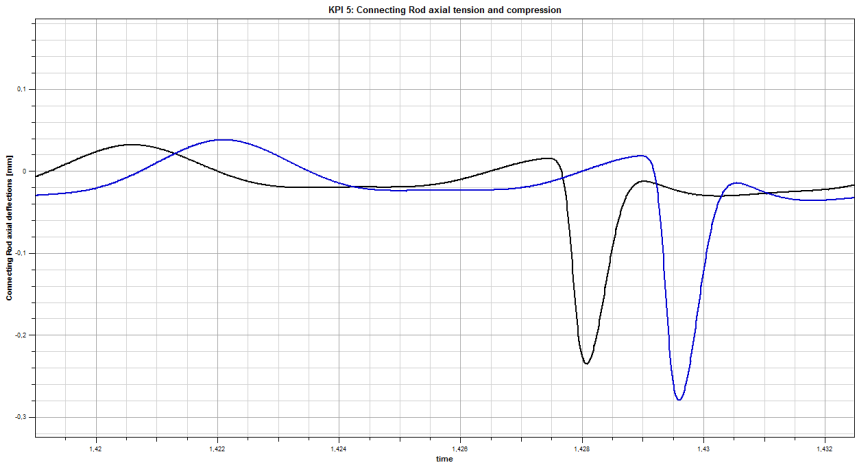

Figure 4.17: Original MXRR rod (blue), New Oval design (black)

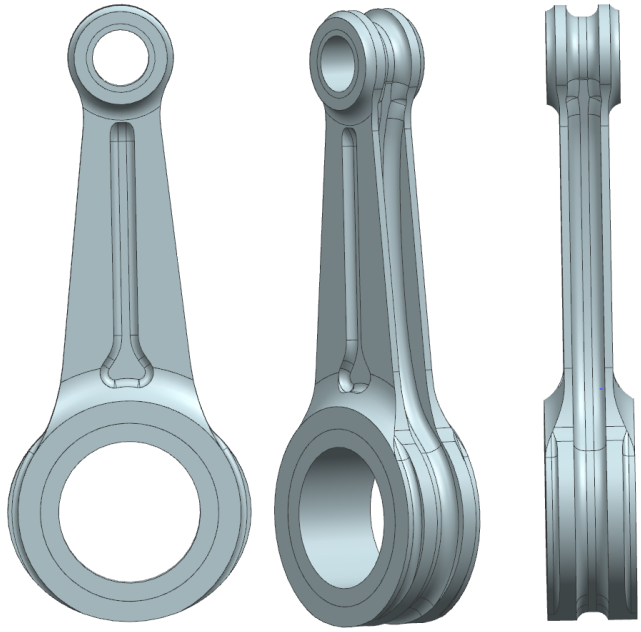

Figure 4.18: Final CRF250L H-Rod design

4.4.3 Piston Pin and Bearing

Total weight optimization in the interlinking parts is governed by both design and material selection. The piston pin is originally made off steel, while MXRR is producing an alternative in titanium and the bearing out of a ceramic material. The mass of the ceramic

material is 0.4 in magnitude relative to steel, while strength is maintained. Presented in figure 4.19 shows that pin weight is almost halved with the improved material. By altering the material in the bearing retainer ring the total weight is reduced by 11.1 grams shown in figure 4.20. Reducing mass in the reciprocating parts of the engine is a positive contribution. With only one cylinder in which it is generated reciprocating forces, there are no other masses to counteract them, as there are in engines with multiple cylinders. Weight reduction in the piston pin is a contributing factor to limit the magnitude of the reciprocating forces, resulting in less severe vibrations.

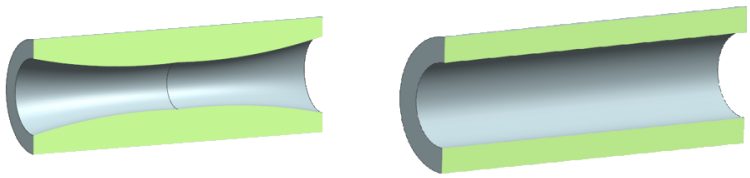

Ceramic Pin weight (g)	Steel pin weight (g)
32	61

Figure 4.19: Piston pin mass and cross section

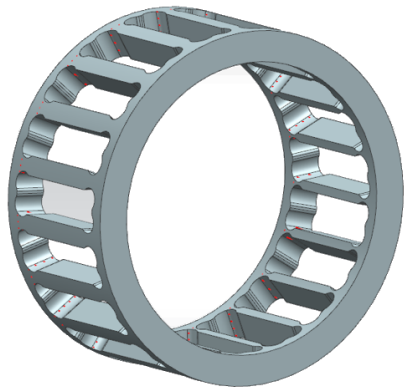

Ceramic Bearing weight (g)	Steel Bearing weight (g)
7.5	18.6

Figure 4.20: Roller bearing retainer masses

4.4.4 Bob Weigths

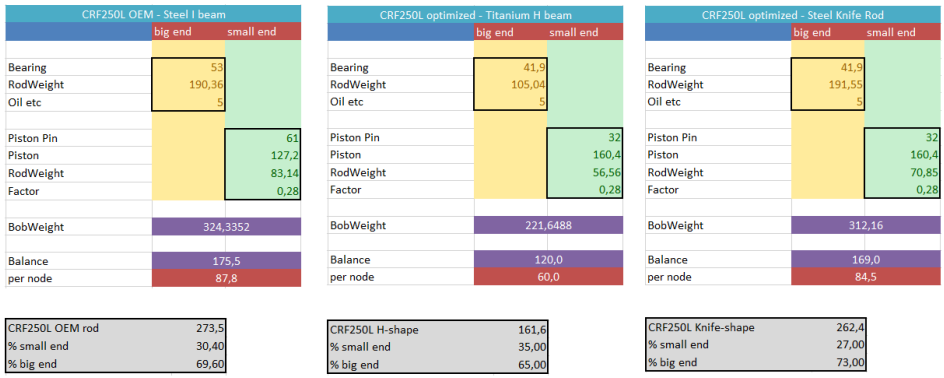

CRF250L OEM - Steel I beam	big end	small end
Bearing	53	
RodWeight	190,36	
Oil etc	5	
Piston Pin		61
Piston		127,2
RodWeight		83,14
Factor		0,28
BobWeight	324,3352	
Balance	175,5	
per node	87,8	

CRF250L optimized - Titanium H beam	big end	small end
Bearing	41,9	
RodWeight	105,04	
Oil etc	5	
Piston Pin		32
Piston		160,4
RodWeight		56,56
Factor		0,28
BobWeight	221,6488	
Balance	120,0	
per node	60,0	

CRF250L optimized - Steel Knife Rod	big end	small end
Bearing	41,9	
RodWeight	191,55	
Oil etc	5	
Piston Pin		32
Piston		160,4
RodWeight		70,85
Factor		0,28
BobWeight	312,16	
Balance	169,0	
per node	84,5	

CRF250L OEM rod	273,5
% small end	30,40
% big end	69,60

CRF250L H-shape	161,6
% small end	35,00
% big end	65,00

CRF250L Knife-shape	262,4
% small end	27,00
% big end	73,00

Figure 4.21: Bob weight sheet

Due to the reciprocating and rotating masses from the connecting rod, piston, piston pin, bearing and bushings, the entire crankshafts are balanced to minimize vibration. Balancing the system will lead to reduced vibrations, in turn affecting performance and engine life. This is especially important in a one cylinder engine as it does not have other offset pistons to counteract the reciprocating forces, resulting in engine vibrations. New bob weights has to be calculated if any of the contributing parts are altered, as total mass and mass distribution differs among the different setups. Achieving a balanced system is done by applying bob weights, placed 180 degrees offset relative to the connecting rod. The forces created by the rotating masses will cancel each other. The way to determine the correct mass starts with determining the center of gravity and calculating the percentage contributing mass of each end of the rod. Then calculating the mass of the required bob weights based on weight percentages and influence factors shown in figure 4.21. Following bob weight calculations are done to each crankshaft setup.

$$BobWeight = (M_{Bigend}) + (M_{Smallend} * 0.28) \tag{4.2}$$

$$Balance = BobWeight * \frac{r_{crankpin}}{r_{bobweigth}} \tag{4.3}$$

The total bob weight is calculated in equation 4.2 summing up the masses of each rod end and its connected parts, which displayed in figure 4.21. To add only the rotational mass a factor of 0.28 is multiplied with small end masses, as these masses mainly move in a linear motion. There are split opinions about the value of this factor, often varying between engine configurations and manufacturers. To obtain the balance weight which is the mass to add to the crankshaft, one has to multiply with a distance contribution

fraction. The fraction consist of the crank pin radius as numerator and bob weight placement radius as denominator, each radius is from center of rotation to placement on the crank. For the CRF250L engine, the fraction is $27.5/83.5$. The bob weights were added in the Fedem software, using zero mass RBE elements from Siemens NX to locate triads with the correct added mass. Observe in figure 4.21 that mass and mass contribution differs between each rod, in addition there are differences in mass of several parts for the different systems.

4.4.5 Mesh

When creating a FEM of the modelled parts there are different considerations to be taken into account. Figure 4.22 show the meshed crank, imported as a single structure into Fedem. The mesh has to be acceptable and give accurate results, in addition 1-D elements has to be added to serve as connecting points for Fedem. Joints, loads or masses require such connecting points. Some of the RBE elements shown with yellow colour in figure 4.23 are used to orient and position the model in Fedem, as it is critical that the whole system lines up. Any misalignment in the system will cause differences and contaminate the results.

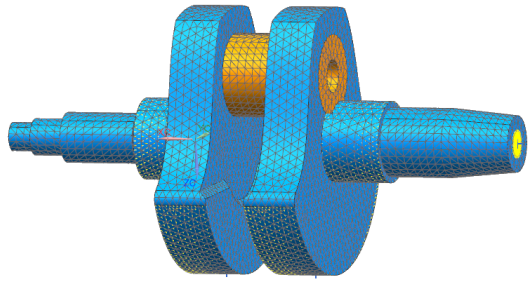

Figure 4.22: Cranskshaft assembly mesh

The connecting rods are meshed with a 3D tetrahedral mesh. Simplified bearings and bushings are mesh mated in the big and small end respectively. Both ends of the rods have 1-D elements as connection points for the Fedem MBS. Conducting a duplicate node check ensures that all meshes are connected. A modal analysis with solver 103 in Siemens NX was performed to further check for meshing errors. In figure 4.24 and 4.25 mesh specifications and parts are displayed. Assigned material data is listed in appendix.

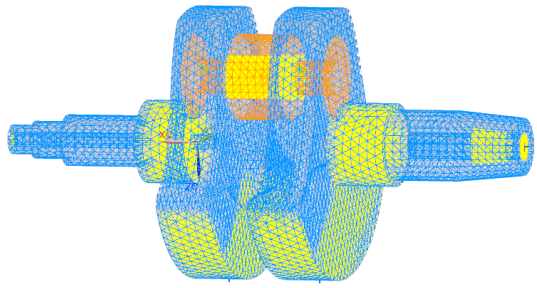

Figure 4.23: RBE element placement

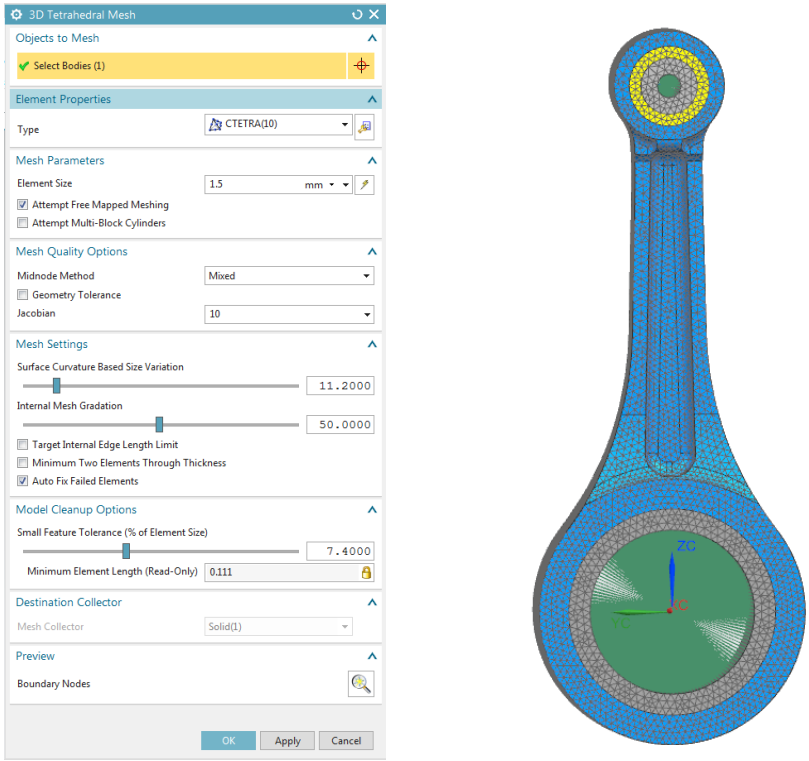

Figure 4.24: Connecting rod FEM mesh and mesh controls

(a) Knife shaped rod mesh

(b) H shaped rod mesh

Figure 4.25: Connecting rod FEM meshes used identical mesh setup as in 4.24

The files were exported from NX to fedem as a .nas file, specifying consistent SI units. The buckling analysis was performed with identical mesh as the Fedem analysis, but RBE elements were deleted. The elements created a artificial stiffness in each end of the connecting rod, leading to large deviations between the linear and nonlinear solver.

Chapter 5

Analysis

5.1 Final System design

By Reverse engineering the existing engine, utilizing performance parts and designing new parts the new engine setup is ready to be analyzed. Total weight difference between the systems is represented in the table 5.1. The three columns show the optimized high-performance engine with titanium H-shaped rod and cermic components, the stock not optimized big bore engine and the OEM setup. By introducing the optimized parts total weight is reduced, though a more powerful engine would generally mean added weight. The only part adding additional mass in the optimized system is the piston due to larger bore. Weight saved in the piston pin is practically the same weight added in the piston, meaning that the masses generating inertia forces should be quite equal between the setups. Total weight reduction on the optimized system is 234.4 g, masses related to the reciprocating parts.

As mentioned in the previous chapter the connecting rods were further developed in this thesis. In figure 5.1 the evolution of rods is presented. To the far left is the oval rod designed by MXRR, it incorporates a shell bearing common in multi-cylinder engines. Even though being the lightest rod at 120 g it was desired to instead incorporate a more durable bearing. The middle rod is the first iteration of a roller bearing rod construction. By increasing the oval big end and shedding weight the rod to the far right was created with a mass of 160.4 g. Being lighter than the OEM and previous iteration rods, it is still heavier than the shell bearing rod as it allows a significantly smaller big end. In a race engine it may make sense to save this amount of weight, as frequent engine maintenance is performed. Ultimately it was decided that the reliability offered by a roller bearing is more important for this machine as it is to be used in everyday application.

Parts	CRF250L High performance	CRF250L not optimized	CRF250L OEM
Crankshaft	2769.1g	2769.1g	2769.1g
Bob Weights	100.4g	182.8g	182.8g
Shims	22.0g	22.0g	22.0g
Crank Pin	407.6g	407.6g	407.6g
Bearing	41.9g	53.0g	53.0g
Conrod	161.6g	273.5g	273.5g
Piston Pin	32.0g	61.0g	61.0g
Piston	160.4g	160.4g	127.2g
Sum:	**3706.1g**	**3940.5g**	**3907.3g**

Table 5.1: Engine setup weights

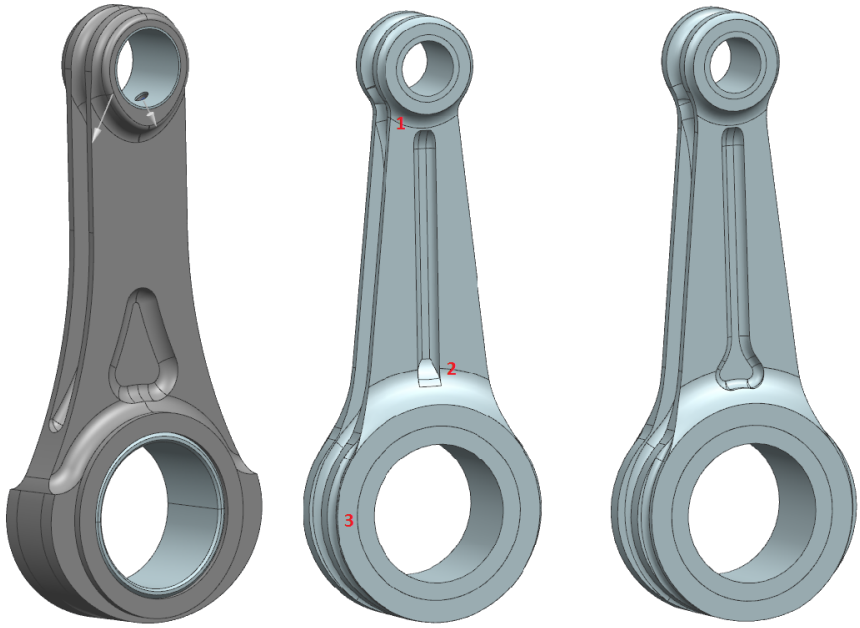

Figure 5.1: CRF250L rod evolving from left to right

5.2 Buckling

The linear buckling simulation was performed with both ends of the rod pinned, allowing rotation, and small end free to move in the loaded direction. Results from this kind of analysis is crude but yield an approximate result. Using the results from a linear buckling solver as a stand alone analysis should only be used if the results are definitively outside the interesting region, like found in the results presented in figure 5.2. As a nonlinear solver is more accurate and takes nonlinear deformation into account, it is the recommended method to obtain correct values. The tree different rods have roughly the same buckling shape, which is to be expected given a similar shape, constraints and load case. Though the titanium H shaped rod differs slightly. In table 5.2 the buckling factors for each rod are recorded, being one to one with applied load.

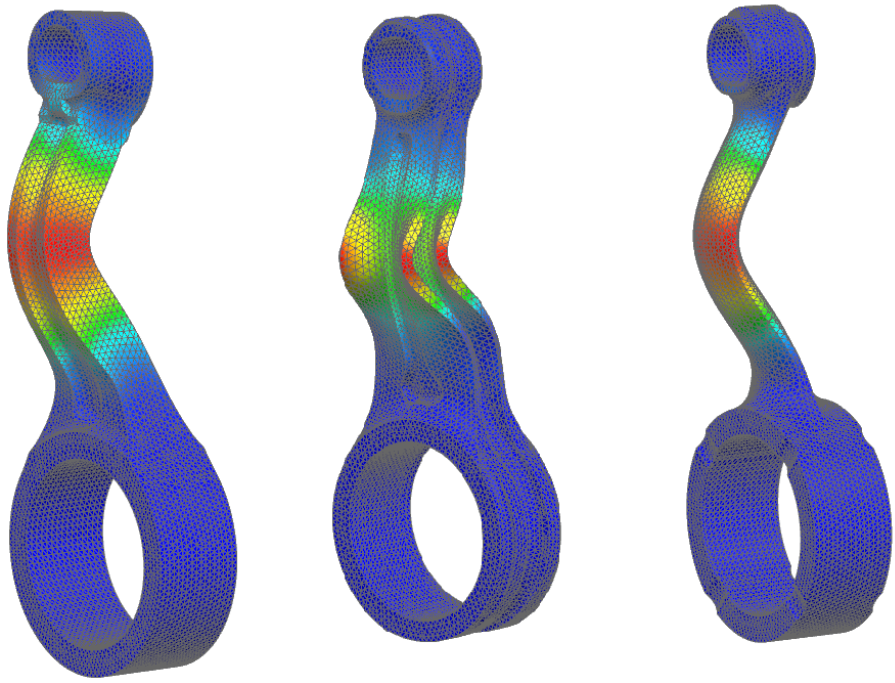

Figure 5.2: Buckling modes from linear buckling solver

	Connecting Rod Masses	
OEM Steel Rod	Steel Knife-Rod	Titanium H-Rod
1696535	847349	616029

Table 5.2: Buckling mode factors corresponding to shapes in figure 5.2

Results from the nonlinear solver show similar shapes and loads. The range of load presented in table 5.3 is far outside any load level generated in the engine. In addition, the stress levels introduced by such a load provokes yield before buckling. The buckling analysis has resulted in conclusive evidence that buckling is not a concern in these three connecting rod designs in normal operation. If severe transverse loads are introduced buckling is more likely. Such extreme loads might be occurring if there are other severe faults within the engine. Examples could be seized pistons or bearings due to overheating or lack of lubrication. There are no available transverse load data, meaning the buckling loads found might be exaggerated. Looking at the load applied to each rod the Knife-shaped rod has the lowest buckling value, and is as heavy as the OEM rod. Leading to the decision to only compare the OEM to H-shaped rod from this point onwards.

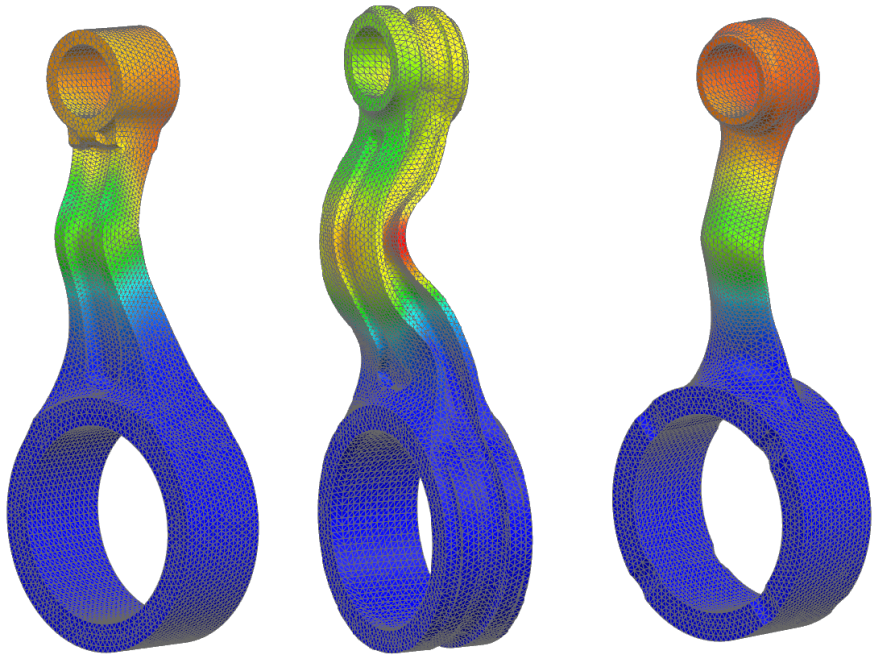

Figure 5.3: Buckling shape from nonlinear solver

	OEM	H-shaped	Knife-shaped
Applied Buckling Load	1700000 N	900000 N	700000 N
Factor	0.9031	0.9375	0.975
Resulting Buckling Load	**1535270 N**	**843750 N**	**682500 N**
Load Initiating Yield	85000 N	90000 N	119000 N

Table 5.3: Output corresponding to shapes in figure 5.3

5.3 Connecting Rod Performance

In figure 5.4 the rpm curves of the optimized and stock engine are plotted. Both engines are driven with the same conditions, the differences in curves is a result of the changes made to the high-performance engine. Lighter components and larger displacement result in a more powerful engine. From time step 1.2 to 1.5 the optimized engine is able to climb a lot higher in rpm, continuing from 1.5 sec the optimized engine also climb steeper until both engines reaches its peak rpm value. Meaning the new engine setup has more power, in this curve throttle response is key. The engines ability to climb in rpm range over time is shown in figure 5.4 both with and without load.

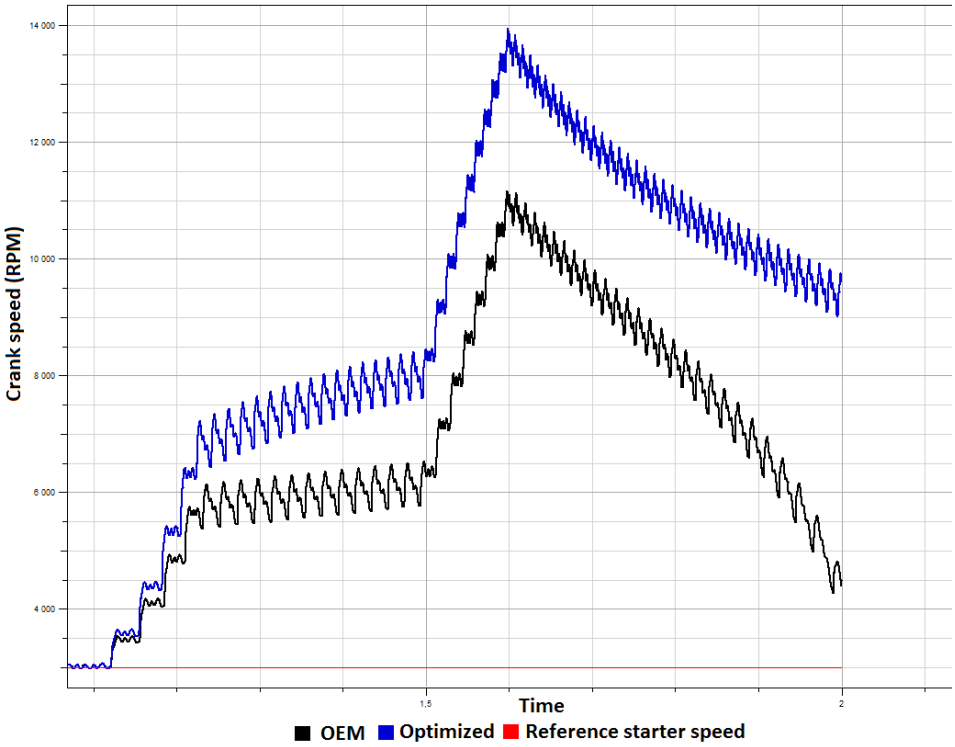

Figure 5.4: RPm Vs Time plot of stock engine (black) and high displacement (blue)

Further backing up the results shown in figure 5.4, can be seen in the effect curve shown in figure 5.5. The recorded in peak effect is 25.5 kW for the high-performance engine and 15.5 kW for the OEM. In horsepower this relates to 34.4 BHP and 20.8 BHP respectively. The control system is made to output about 21 BHP in the OEM setup. Introducing the bigger piston and optimized parts result in an increase in power of 13.6 BHP. The increase in effect is due to pressure function working on the larger piston area, also contributing is the new lighter components. With this setup the relation between the two engines is true and indicates how the cylinder pressure relates to effective area of the piston.

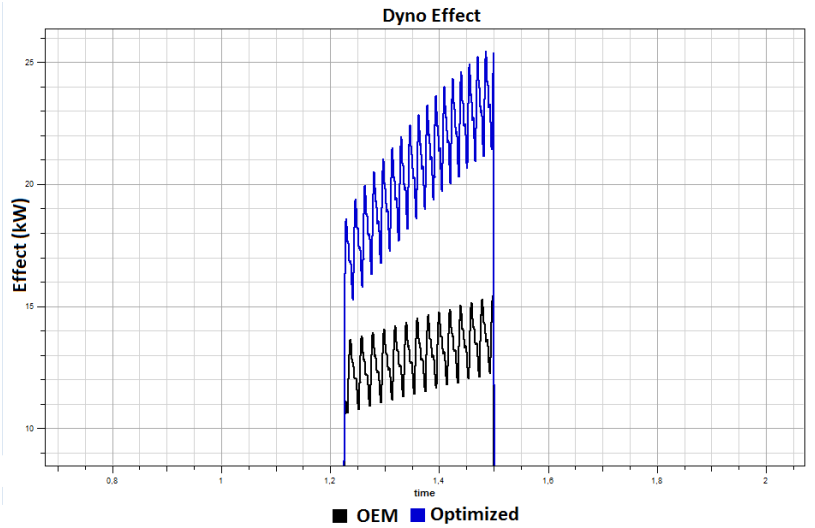

Figure 5.5: Effect curves, OEM vs Optimized

The following results are recorded for the bigger displacement engines, the two different setups are with stock components vs new optimized components. The two setups are visualized from Fedem in figure 5.7 and the respective masses are shown in column 1 and 2 in table 5.1. As presented by the plotted curves in figure 5.6 the two curves show a significant difference between them. The only thing contributing to the differences is the changes introduced by replacing parts. The differences in masses is clearly affecting the system, where the optimized and lightest setup is able to reach a higher rpm range.

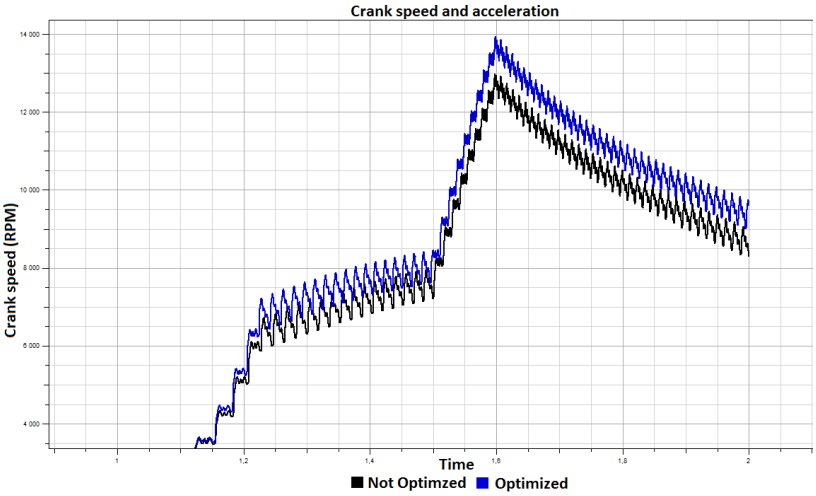

Figure 5.6: Effect vs Time for OEM engine (black) and optimized engine (blue) both with high displacement piston and bore

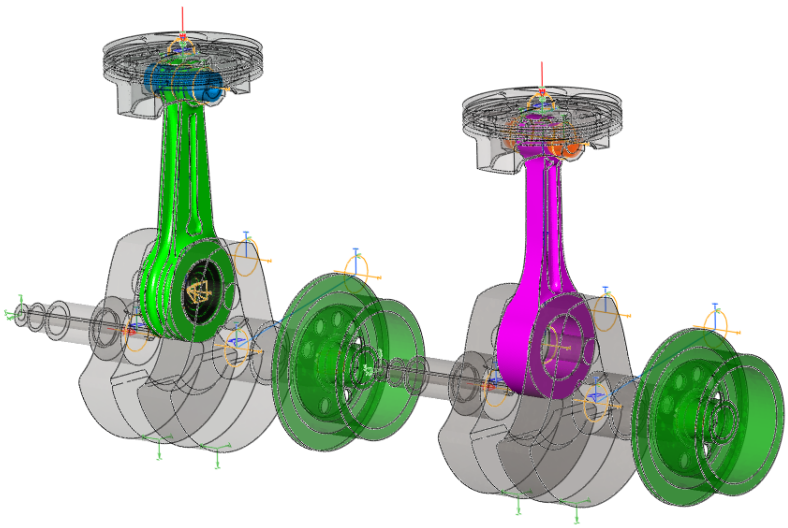

Figure 5.7: Fedem model component overview

5.4 Maximum Compression Stresses

Piston forces are plotted in figure 5.8, the force is a result of combustion in the power stroke. The forces have equal maximum values peaking at 50 kN found in the areas indicated with red circles. The highest combustion forces are found when the engine is under load, as the crankshaft has maximum resistance from the driveshaft. Forces are slightly shifted in the plot as the two engines rev at different speeds, as the two systems does not have equal contributing masses. In comparison to the results found in 5.8 the maximum piston force with the stock engine with smaller piston was 45 kN.

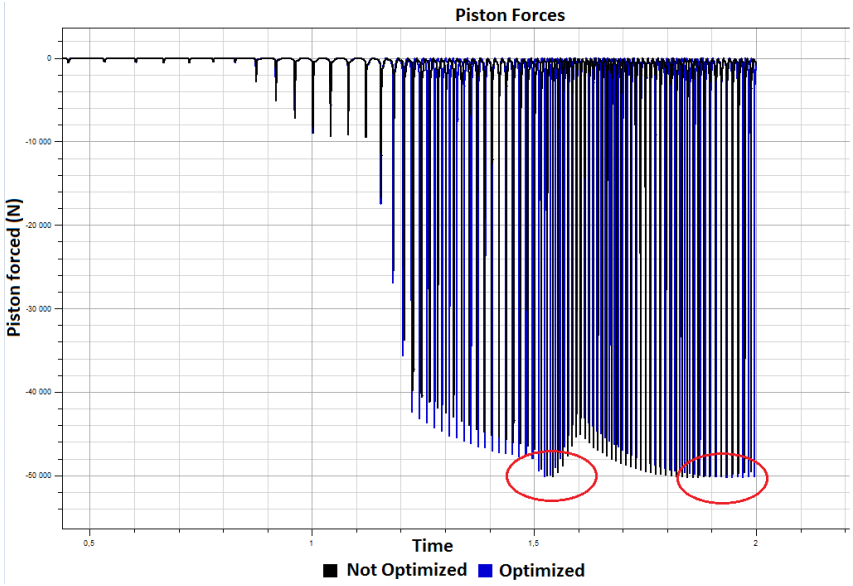

Figure 5.8: Piston force generated from combustion

Stress distribution in figure 5.9 is collected at maximum piston force indicated with the red circle in figure 5.8 at around 1.5 seconds. To ensure maximum stresses, the deflection curve were used to probe at the point of maximum deflection within the area of maximum piston force, curve shown if figure 5.9. The contour plot show lower stress levels in the new rod for the total geometry . By looking at the shank of the rods, the new titanium rod has similar stress levels all along the shank but significantly lower in the neck and big end area. It looks like dramatic changes in the contour plot, but the OEM steel rod is far from close to yielding. The legend scale has been made to highlight the present stresses.

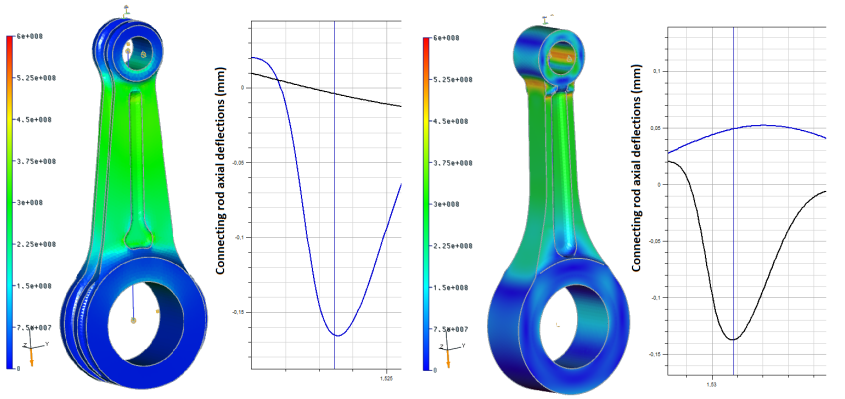

Figure 5.9: Maximum compression stresses found in maximum compression

A closer look at the ends of the rod reveals significantly lower stresses for the optimized rod. Hotspot stresses are present at the small en of the OEM rod, however the new connecting rod has a more uniform distribution. Highest stresses found in the new rod is peaking at 390 MPa while the old rod has peak values at 688 MPa. These peak values should not be the focus, as values are found at hard edges and corners, removing blends and chamfers in the idealization phase may have lead to exaggerated values in certain areas. Rahter one should focus on the general stress distribution, which seems more beneficial for the titanium rod. As found in the preliminary project paper hoop stresses are reduced by increasing the lateral sides of the big end. The optimized rod in figure 5.10 show the same results, with low hoop stresses, while still maintaining the possibility to incorporate a roller bearing. With a single cylinder engine, a monolithic rod construction with a durable bearing makes sense, as it reduces amount of components and increases strength.

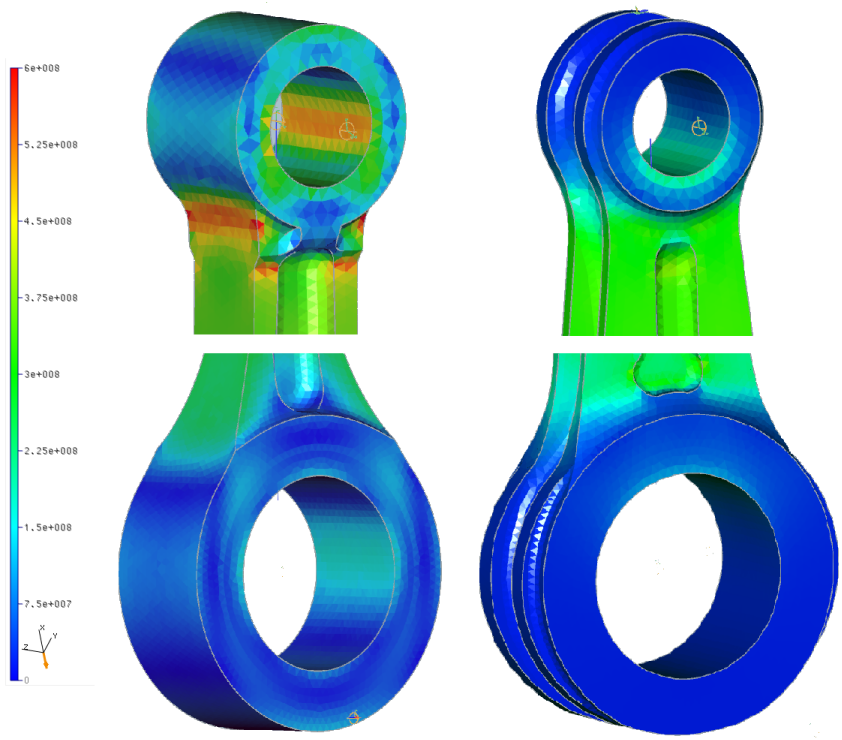

Figure 5.10: Maximum compression stresses in rod ends

5.5 Maximum Tension Stresses

Tension stresses are a key part of the stress cycle rods endure. In the exhaust stroke there is low resistance in the cylinder as the exhaust valve is open. As the piston reaches top dead center in the exhaust stroke, inertia forces play a vital role, generating tension stresses.

In figure 5.11 the piston inertia forces are plotted. The shape of the curve follows the rpm curve shown in 5.6, as the angular velocity of the crankshaft dictates the translational velocity of the rod and piston. As the crankshafts reach maximum rpm the pistons reach maximum velocity, and in turn highest inertia forces.

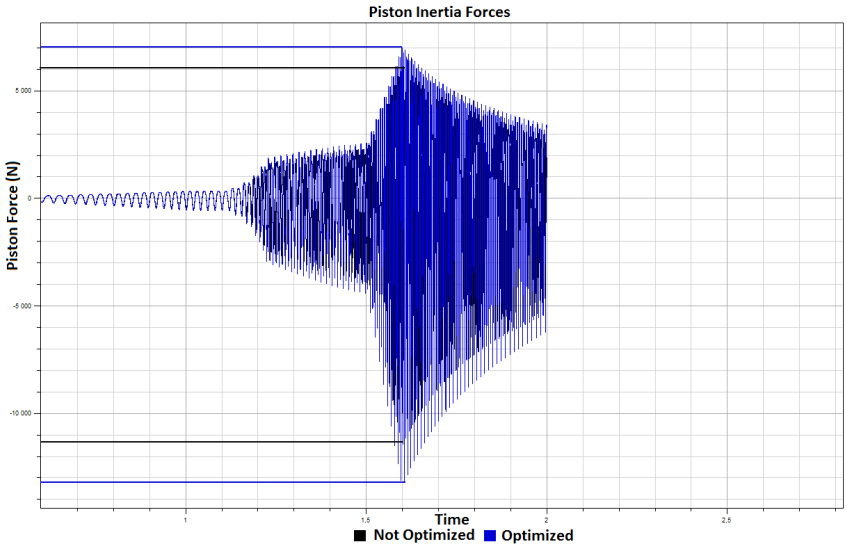

Figure 5.11: Inertia forces

From the rpm curve in figure 5.6 and the inertia force in figure 5.11 we see that highest rpm range coincide with highest inertia force at 1.6 seconds. Peak Piston inertia forces is found to be 7 kN for the new rod, and 6 kN for the old rod, shown in figure 5.11 with blue and black respectively. One should expect higher inertia forces in the black curve as the crankshaft has a higher connected mass, but the highest force value is found in the new setup. The reason being that the new optimized engine operate at higher rpm, which increase piston velocities, and in turn inertia forces.

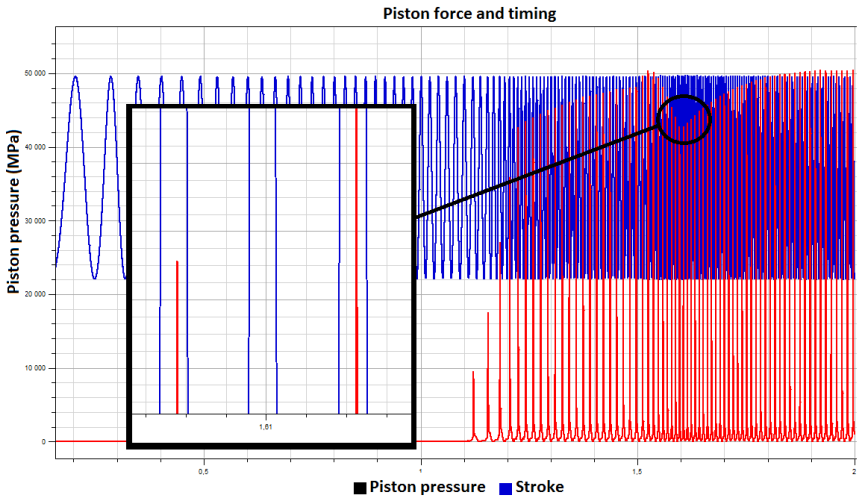

Figure 5.12: Force (red) and stroke (blue) plotted to identify combustion and exhaust strokes and timing

Highest inertia forces is found at 1.61 seconds as shown in figure 5.11. At this time a dead stroke occurs shown in figure 5.12. The red curve shows piston combustion forces, and the blue line is piston position or stroke. As each surrounding curve peak has a combustion force, the stroke happening at 1.61 does not and is an exhaust stroke. The deflections occurring at this instance is also peaking. Figure 5.13 contain both rod deflection peaks in tension.

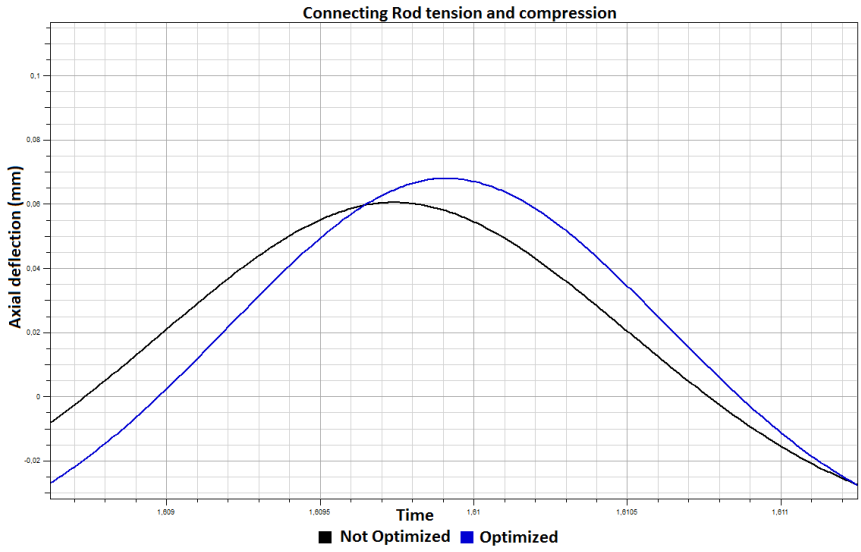

Figure 5.13: Maximum deflection in tension

The stress distribution from the current time increment is presented in figure 5.14. The fringe range is modified to highlight stress differences. Highest stresses found in tension is given in the figure, the maximum stress occurring in the new rod is 151 MPa, and 337 MPa for the OEM steel rod. Again we can look at the ends of the rods, clearly showing lower stresses for the new improved titanium rod. Due to the oval design stresses are reduced, and so will the stretching and ovalization of the rod.

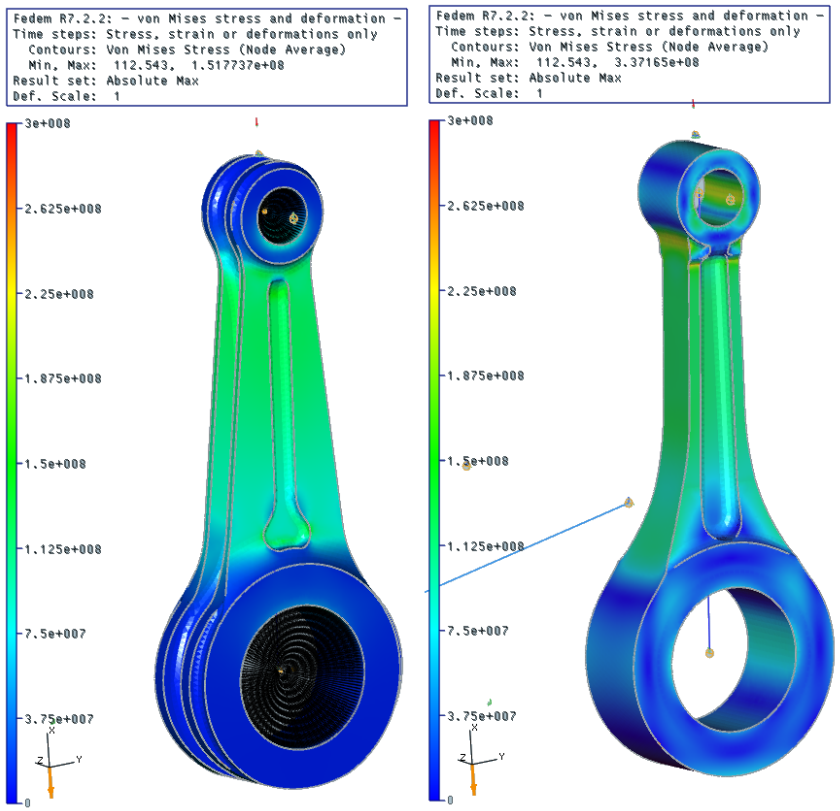

Figure 5.14: Stresses found in maximum tension

5.6 Axial Displacement

The curves given in 5.15 and 5.16 are the axial displacement of the rods in mm. Maximum compression resulting from combustion forces and tension from inertia forces. The data presented from the curves are obtained through an axial displacement sensor in Fedem, connected between big and small end of the rods. Positive values refer to amount of stretch and negative values to compression.

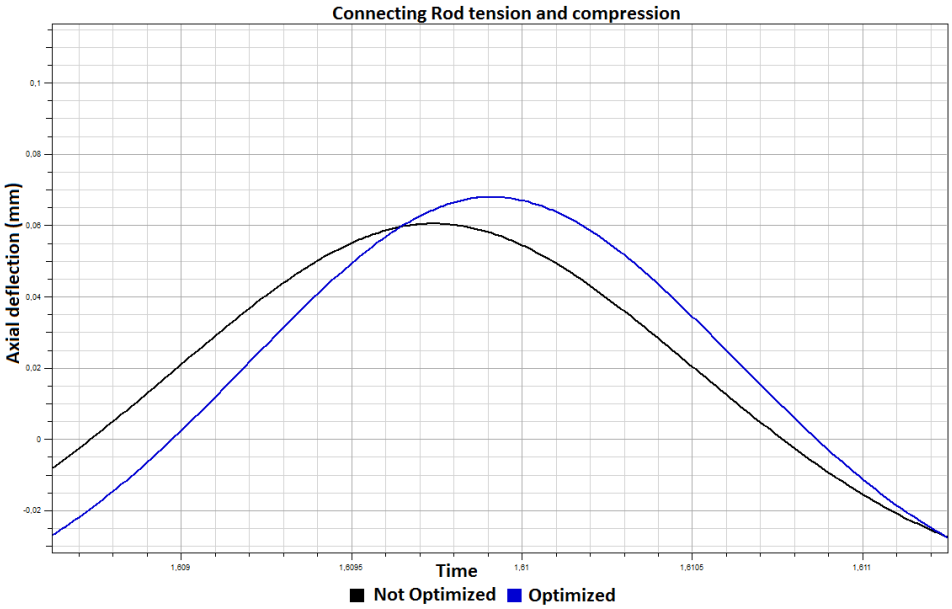

Figure 5.15: Maximum deflection in tension

In tension we find the smaller deformations as opposed to compression. Which is expected, as forces in tension is smaller. As seen in the previous section, figure 5.15 display the maximum tension deformation. Maximum elongation is found at maximum rpm, around 1.6 seconds. At this moment components are traveling at maximum velocities, being a driving factor for increasing inertia loads. Values for the new and OEM rod is 0.07 mm and 0.06 mm respectively. In comparison to the OEM rod under OEM performance condition the maximum elongation is 0.045 mm. While the OEM rod has smaller deflections, but largest stresses is caused by difference in stiffness, titanium has a Young's modulus of 1.2e11 Pa and steel is 2.06e11 Pa. Contributing to the fact that the new rod has a better geometric shape to handle the stresses, as it is subjected to the highest loads, and keep the stress levels low.

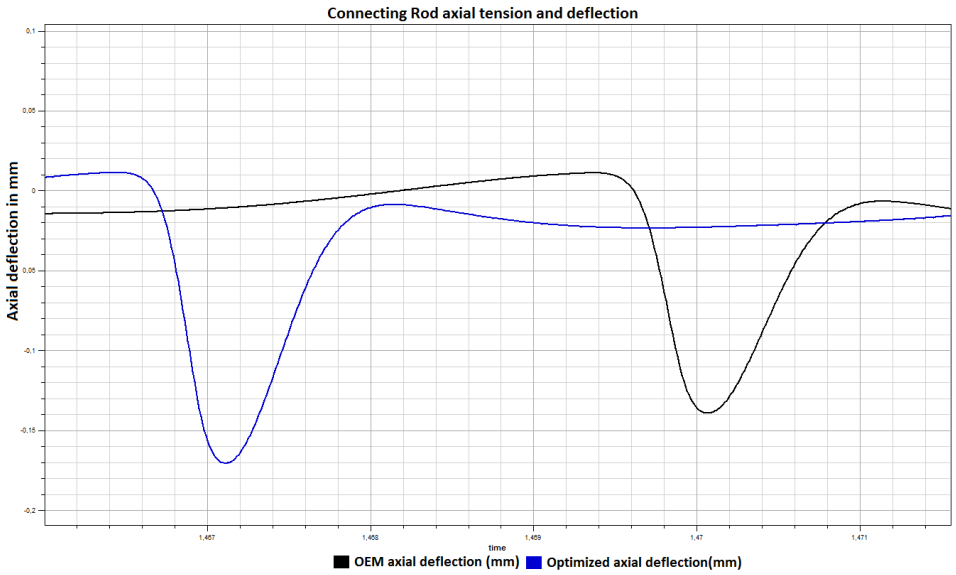

Figure 5.16: Maximum deflection in compression

In compression larger displacements are found. The titanium rod compresses by 0.17 mm and the OEM rod by 0.14 mm. Again, we see that the new setup deflects more. From the results of the CRF250R engine performed in the preliminary project paper, rods deflect nearly 50 % more. These rods are also shorter resulting in even higher percentage wise elongation, suggesting that the deformations we see in the rods presented in this thesis is an improvement. As mentioned the titanium rod does deflect more than the OEM steel rod, though it is important to remember that while the compression force is equal, the inertia forces are not. The New rod is moving faster than the old, contributing to deflecting the rod. The difference is correct and should be respected, mind only that the new rod has to withstand higher forces.

The new and improved titanium rod is effectively reducing deformations. Before removing material in the shank and adding oval strengtheners the deflections was as 0.24 mm in compression and 0.10 mm in tension. The two different designs are shown in figure 5.17, the numbers found on the first iteration rod is the areas to be improved. The final design to the right has had material added below the small end at point 1. In the shank, material has been removed to save weight and contribute to stress flowing on the lateral sides of the rod. In point 3, the lateral oval ribs has gotten a lager lateral diameter to avoid ovalization. These three points of improvement contribute to reduced stress concentrations and in turn smaller deformations.

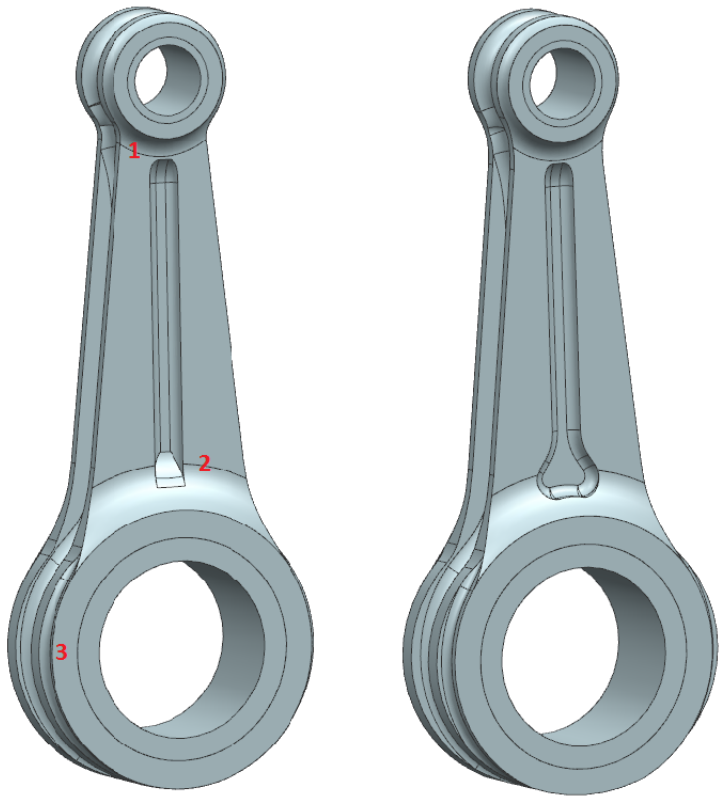

Figure 5.17: Final alterations of the connecting rod in areas shown from 1-3

Chapter 6

Discussion

While the results are discussed in the previous chapter, some aspects of the paper deserve extra attention. The modifications made to the CRF250L engine that has had most influence on results is discussed more closely in this chapter. In addition, take a closer look at the given tasks to solve.

- Reverse engineer the stock HONDA CRF 250L engine.
- Design an optimal connecting rod type based on Falicon or MXRR CRF250R designs. Optimize the rod for the desired CRF250L performance.
- Select an optimal piston pin and bearing from MXRR for the wanted CRF250L performance.
- Identify load cases / KPIs (max compression and tension) in the FEDEM test bench to quantify the structural integrity of all critical engine components on the stock and optimized CRF250L engines.

6.1 Fedem

Utilizing the Fedem testbench to analyze engine components has been the foundation for design alterations. Initially the testbench was intended for the CRF250R engine but whas been rebuilt for the CRF250L engine. All internal parts have been exchanged as the two engines despite similar name, do not share any common parts. By carefully replacing parts and making sure everything is in line the new engine was constructed. Due to lacking information and physical parts some assumptions have been done. Information from the workshop manual and the reverse engineered parts are the only source of decisive information to the internal components and characteristics of the engine. As previously mentioned, the pistons were not possible to obtain. The CRF250R piston has been altered to meet the critical dimensions of the CRF250L engine. The same procedure has had to be done with piston pin, balancer and flywheel. All components are shown in figure 4.9.

The control system is another part that has been necessary to approximate. The pressure cycle has been reworked from the CRF250R cycle. Pressures in figure 4.11 has been altered to generate correct power, but timing is kept unaltered. These measures introduce differences between the analysis setup and the real-life case. Care has been taken to reduce the difference as much as possible, given the conditions. Knowing that the results are unable to reproduce the exact real-life conditions, the results gathered is not focused on the peak stress or maximum rpm. The most important and useful results gathered is the improvement between the two side by side crankshafts in Fedem. By performing the analysis side by side, the differences between optimized and unoptimized system become evident. Keeping stress and strain levels below or equal to the Stock OEM engine indicate that components are structurally sound and reliability is maintained. The improvements are portrayed in the previous chapter and can be regarded as conclusive results of what changes in different engine components contribute to in regards of engine performance.

6.2 Connecting Rod Selection

The knife shaped rod was rejected quite early in the process and was not tested in Fedem. The specific design was provided by Falicon racing. Initially it seemed to be an ideal connecting rod. The material properties were superior for a steel with yield strength of 2500 MPa. Proving to be the rod to endure the highest compressive loads before yield, seen in table 5.3. As the CRF250L is a fairly low performance engine, even with the higher displacement piston the Falicon rod is made for higher output engines. Comparing weight to the original rod, it is only a minimal difference. When the titanium H-shaped rod was compared to the Falicon rod it did not make sense to pursue the steel alternative, as weight reduction was improved while maintaining a structurally sound geometry.

Maintaining low weight in moving components proved to be beneficial, reducing inertia forces and improving performance. To utilize lighter materials in components and a more beneficial design yielded a lighter overall system. While reducing weight proved beneficial, the results suggested that mass close to the crankshafts rotational axis is of less importance to performance. In figure 6.1 one can see the connecting rod centerline is perpendicular to the crankshaft center of rotation, mass close to this axis has low inertia and is regarded as a rotational mass. Mass further away from the crankshaft rotational axis in the connecting components is contributing to reciprocating mass, introducing inertia forces and vibration in single cylinder engines. Keeping the necessary masses close to center of rotation and reducing overall weight has contributed to the results shown in the previous chapter. In table 5.1 component masses are presented, placement of the improved upon masses are shown in figure 6.1. In point 1 the piston and piston pin are mounted, the added weight caused by a bigger piston is counteracted by the piston pins reduced weight. As the piston has its center of gravity further from the axis of rotation than the piston pin and adding a small additional mass to the system, it is by itself a factor expected to increase inertia forces on the system. Point 2 is the connecting rod, reduced weight in this component is significant. In figure 4.21 the weight and distribution can bee seen, one thing to note is the weight percentages contributing to each end. To further improve this rod design, it could be beneficial to reduce small end mass percentage value and increase

big end value, to move masses closer to rotational center. Point 3 relates to the bearing mass, not the biggest or most important weight saving measure but maintaining a roller bearing in the big end is a way of maintaining engine reliability. Point 4 is bobweight placement, all other mass reductions are the basis for reducing bobweight mass. In this instance it has been decided to move the bobweight mass as far from the rotational axis as possible, to introduce as little mass as possible. The placement of bobweights for from the center is not only to reduce added mass, but also due to dimensional reasons.

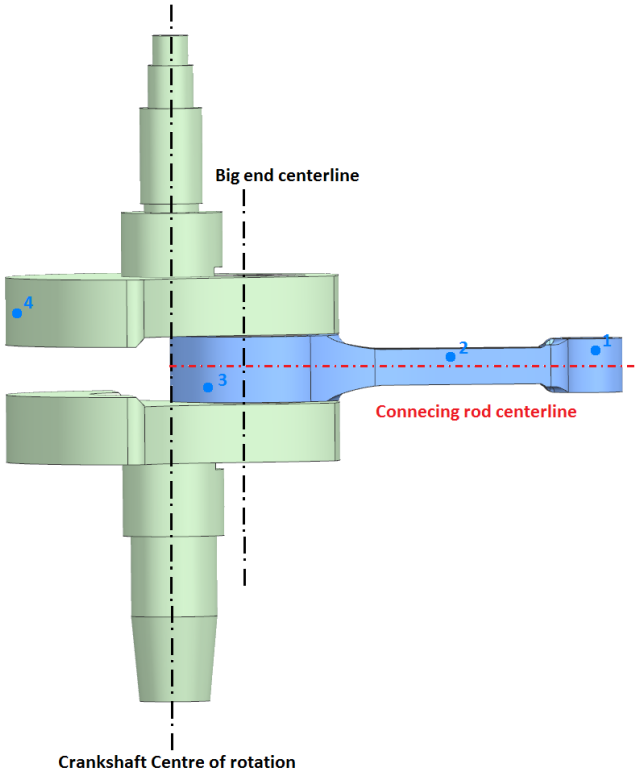

Figure 6.1: CRF250L crankshaft

Increasing the wings of the big end of the connecting rod proved to reduce stresses and ovalization in the big end. As found in the preliminary project paper the reduction in deflection is significant when the lateral sides of the big end are improved. It was found in the preliminary project paper that the deflection reduction shown in figure 4.17 is solely due to an improved big end design shown in figure 4.16b. It was concluded that ovalization has a significant contribution to connecting rod deflection in tension and compression. By only altering the big end design, it was possible to pinpoint the exact region of the rod to change. The model shown in figure 4.16b was initially created to withstand forces produced from the CRF250R engine, with a power output twice whats found in the CRF250L. The new connecting rod based on the MXRR design is presented in figure 6.2. Smaller

lateral wings highlighted with red were used to reduce ovalization. Excessive material was reduced, due to the lower power output engine. In addition, the design had to be altered to accept a roller bearing, requiring an overall larger big end. As mentioned in previous chapter titanium has a lower stiffness than steel. Larger deformations occur under same load, and specific design features must be introduced. The main features are H-shaped shank and an oval big end.

Figure 6.2: CRF250L Connecting rod design

6.3 Key Performance Indicators

As mentioned earlier in this chapter, the most important results are the evolving performance upgrades. The KPIs suggested in this thesis are ment to both capture relevant information from the Fedem analysis setup shown in figure 4.10 and provide a basis to compare the two different engine setups. The results provided in the previous chapter is made to highlight the important differences introduces by optimization. The chosen key performance indicators are based on real life events putting high strain on the engine. By testing worst case conditions under normal engine operation, it is assumed that if the engine is able to handle these, all other normal engine operation conditions is unproblematic. While focusing on the differences between systems rather than extreme values of stress, strain or rpm. There are other factors to be considered in engine optimization not included in this thesis, such as lubrication, heat dissipation and fatigue.

6.4 Concluding Remarks

In this master thesis performance upgrades of the CRF250L engine has been studied. Performance and durability are improved by increasing engine displacement to $305cm^3$ and upgrading internal engine components. The focus has been on the crankshaft and connecting components, with the intent to optimize them for higher performance output. The three different rod designs presented in this paper was analyzed in Siemens NX and Fedem. Buckling analysis in Siemens NX show that buckling is unlikely under normal operation. The New titanium rod design proved the most beneficial of the tested rods. Reducing weight and showing smaller stresses than previous rods. The alterations done to this rod has resulted in less rotational and translational mass, with great structural integrity and the incorporation of a roller bearing to improve durability. Adding material to the lateral sides of the big end of the rod reduced axial displacement induced by ovalization, though minimizing material at strategic areas kept weight low. When strengthening the big end the added mass proved to have a small impact on performance, reason being that the mass is close to the crankshafts center of rotation. By pairing the new high displacement engine with ceramic bearings, titanium piston pin and connecting rod a lightweight system was obtained, requiring less additional mass in bob-weights as can be viewed in table 5.1 and 6.1. The new improved engine assembly has had a significant power upgrade, while handling introduced load levels. Showing smaller stresses, which increase reliability.

Parts	CRF250L High performance
Crankshaft	2769.1g
Bob Weights	100.4g
Shims	22.0g
Crank Pin	407.6g
Bearing	53.0g
Conrod	161.6g
Piston Pin	32.0g
Piston	160.4g
Sum:	**3706.1g**

Table 6.1: Final crankshaft setup

6.5 Further Work

To further improve upon the current CRF250L design more parts must be reverse engineered. A complete engine should be acquired to not only look at specific parts by themselves but optimizing them simultaneously. In chapter 2 several possible engine components that could be optimized are presented. The revered engineered components presented in this master thesis also could be improved upon, especially the crankshaft itself which is a roughly made part compared to the similar CRF250R crankshaft. There is certainly many possible routes to further improve the CRF250L engine, but cost has to be taken into account. The CRF250L is a low-cost motorcycle it does not make sense improving upon

parts that is going to be too costly to implement. Also keeping in mind that these bikes are used as daily drivers and commuter bikes, keeping them reliable and easy maintained could be challenging if performance increasing measures is taken too far.

Bibliography

Encyclopdia-Britannica-Inc, 2018a. accessed 1 September 2018. https://www.britannica.com/technology/slider-crank-mechanism/media/548729/7447.

Encyclopdia-Britannica-Inc, 2018b. accessed 25 Aug 2018. http://media.web.britannica.com/eb-media/72/93572-034-26C16785.jpg.

Fedem-Technology-AS, 2016. Fedem Release 7.2 Theory Guide. Fedem Technology AS.

Hammil, D., 2005. Camshafts and Camshaft Tuning for High Performance Engines. Veloce Publishing Ltd.

Honda-Motor-Co., 2013. Honda CRF250L workshop manual. Honda-Motor-Co.

Meng, X., Ning, L., Xie, Y., Wong, V. W., 2013. Effects of the connecting-rod-related design parameters on the piston dynamics and the skirtliner lubrication. Journal of Automobile Engineering 227 (6), 885–898.

Moon, H., Shin, S., Chang, H., Lee, K., Yeom, D., 2007. Development and application of buckling estimation method in engine connecting rod. SAE International 0148-7191.

Rølvåg, T., Bella, M., 2017. Dynamic test bench for motocross engines. Advances in Mechanical Engineering 9 (10), 1–19.

Strozzi, A., Baldini, A., Giacopini, M., Bertocchi, E., Mantovani, S., 2016. A repertoire of failures in connecting rods for internal combustion engines, and indications on traditional and advanced design methods optimal control theory. Engineering Failure Analysis 60 (4), 20–39.

Appendix

Table 1. Baseline engine data.

Symbol (units)	Definition	Value
a (mm)	Vertical position of the COM of the piston	−1.737
b (mm)	Vertical position of the center of the piston pin	11.8
C (mm)	Nominal radial clearance between the piston and the bore	0.015
C_g (mm)	Horizontal distance between the COM of the piston and the piston pin	0.13
C_p (mm)	Piston pin offset	0.7
I_{ps} (kg m^2)	Rotational inertia of the piston	1.29×10^{-4}
I_R (kg m^2)	Rotational inertia of the connecting rod	9.67×10^{-4}
j	Location of the COM of the connecting rod (ratio, $0 < j < 1.0$)	0.22
L (mm)	Length of the piston skirt	28
l_c (mm)	Length of the connecting rod	129.5
m_{ps} (kg)	Mass of the piston	0.19
m_{pin} (kg)	Mass of the piston pin	0.074
m_R (kg)	Mass of the connecting rod	0.345
R (mm)	Radius of the Piston	36.485
r (mm)	Crankshaft radius of gyration	39.93
α_1 (deg)	Angle of half the bearing area of the skirt's TS	46
α_2 (deg)	Angle of half the bearing area of the skirt's ATS	46
η (Pa s)	Viscosity of the lubricant	0.01

COM: center of mass; TS: thrust side; ATS: anti-thrust side.

Meng et al. (2013)

MATERIAL INFORMATION

Library Material : TitaniumMXRRMassless Category METAL Library Reference Titaniummassless.xml Category : METAL Sub-Category : Titanium Alloy Alternate Name : Not Defined Mass Density (RHO) : 1kg/m

======== Mechanical Young's Modulus (E) : 110000000kPa : 0 Poisson's Ratio (NU) : 0.34 Stress-Strain Input Data Type : 0 Type of Nonlinearity (TYPE) : 1 Yield Function Criterion (YF) : 1 Hardening Rule (HR) : 1 Mechanical Power to Heat Ratio : 0

======== Strength Yield Strength : 862000kPa Ultimate Tensile Strength : 960000kPa

======== Durability Stress-Life Data : 0 Fatigue Strength Coefficient : 1293000kPa Fatigue Strength Exponent : -0.088 Strain-Life Data : 0 Fatigue Ductility Coefficient : 0.26 Fatigue Ductility Exponent : -0.721 Percent Reduction in Area : 0 R-Ratio : 1 : -1 Test Type : 0 Survival Probability : 50 Tsigma (90/10) : 1.5 : 0

======== Formability Initial Strain : 0.02mm/mm Hardening Exponent : 0.2 Strength Coefficient : 1449.277MPa R0 : 1.4 R45 : 1.5 R90 : 1.7

======== Thermal/Electrical Thermal Expansion Coefficient (A) : 8.6e-06C Thermal Conductivity (K) : 6700W/(mmC) Specific Heat (CP) : 526000000J/(kgK)

======== Creep : 0

======== Viscoelasticity Model : 0

======== Viscoplasticity Viscoplastic Type : 0

======== Damage : 3

======== Miscellaneous Crosshatch Pattern : Refractory Fixed Stock Thickness : 0 Adhesive : Not Defined Adult HIC1000 Offset : 95mm Adult HIC1700 Offset : 74mm Child HIC1000 Offset : 85mm Child HIC1700 Offset : 68mm Leg Impact Offset : 50mm NCAP Adult 650 Offset : 115mm NCAP Child 650 Offset : 105mm NCAP Adult 1000 Offset : 94mm NCAP Child 1000 Offset : 90mm NCAP Adult 1350 Offset : 74mm NCAP Child 1350 Offset : 70mm NCAP Adult 1700 Offset : 65mm NCAP Child 1700 Offset : 60mm

MATERIAL INFORMATION

Library Material : TitaniumMXRR Category METAL Library Reference TitaniumMXRR.xml Category : METAL Sub-Category : Titanium Alloy Alternate Name : Not Defined Mass Density (RHO) : 4.43e-06kg/mm

======== Mechanical Young's Modulus (E) : 110000000kPa : 0 Poisson's Ratio (NU) : 0.34 Stress-Strain Input Data Type : 0 Type of Nonlinearity (TYPE) : 1 Yield Function Criterion (YF) : 1 Hardening Rule (HR) : 1 Mechanical Power to Heat Ratio : 0

======== Strength Yield Strength : 862000kPa Ultimate Tensile Strength : 960000kPa

======== Durability Stress-Life Data : 0 Fatigue Strength Coefficient : 1293000kPa Fatigue Strength Exponent : -0.088 Strain-Life Data : 0 Fatigue Ductility Coefficient : 0.26 Fatigue Ductility Exponent : -0.721 Percent Reduction in Area : 0 R-Ratio : 1 : -1 Test Type : 0 Survival Probability : 50 Tsigma (90/10) : 1.5 : 0

======== Formability Initial Strain : 0.02mm/mm Hardening Exponent : 0.2 Strength Coefficient : 1449.277MPa R0 : 1.4 R45 : 1.5 R90 : 1.7

======== Thermal/Electrical Thermal Expansion Coefficient (A) : 8.6e-06C Thermal Conductivity (K) : 6700W/(mmC) Specific Heat (CP) : 526000000J/(kgK)

======== Creep : 0

======== Viscoelasticity Model : 0

======== Viscoplasticity Viscoplastic Type : 0

======== Damage : 3

======== Miscellaneous Crosshatch Pattern : Refractory Fixed Stock Thickness : 0 Adhesive : Not Defined Adult HIC1000 Offset : 95mm Adult HIC1700 Offset : 74mm Child HIC1000 Offset : 85mm Child HIC1700 Offset : 68mm Leg Impact Offset : 50mm NCAP Adult 650 Offset : 115mm NCAP Child 650 Offset : 105mm NCAP Adult 1000 Offset : 94mm NCAP Child 1000 Offset : 90mm NCAP Adult 1350 Offset : 74mm NCAP Child 1350 Offset : 70mm NCAP Adult 1700 Offset : 65mm NCAP Child 1700 Offset : 60mm

---

MATERIAL INFORMATION

Library Material : Moldstar 22 Category METAL Library Reference Moldstar22.xml Category : METAL Sub-Category : Alloy Steel Alternate Name : Not Defined Mass Density (RHO) : 7.058e-06kg/mm

======== Mechanical Young's Modulus (E) : 214000000kPa : 0 Poisson's Ratio (NU) : 0.3 Stress-Strain Input Data Type : 4 Stress-Strain (H) : Tabular Data: strain Stress-Strain (H) mm/mm kPa 0 0 0.00114 235000 0.0296 237000 0.0392 255000 0.0488 270000 0.0583 283000 0.0677 295000 0.077 306000 0.0862 315000 0.0953 323500 0.1044 331500 0.1133 338500 0.1222 343500 0.131 348000 0.1484 356500 0.157 360500 0.1655 364200 0.174 367500 0.1823 370500 0.2 376700 0.3 406000 0.4 430000 0.5 450000 0.6 468000 0.7 483000 0.8 496000 0.9 508000 1 520000 Type of Nonlinearity (TYPE) : 1 Yield Function Criterion (YF) : 1 Hardening Rule (HR) : 1 Initial Yield Point (LIMIT1) : 235000kPa Mechanical Power to Heat Ratio : 0

======== Strength Yield Strength : 235000kPa Ultimate Tensile Strength : 340000kPa

======== Durability Stress-Life Data : 0 Strain-Life Data : 0 Percent Reduction in Area : 0 R-Ratio : 1 : -1 Test Type : 0 Survival Probability : 50 Tsigma (90/10) : 1.5 : 0

======== Formability Work Hardening : 0.22 Forming Limit : Tabular Data: temperature Forming Limit C Unitless -0.5 0.88 0.02 0.35 0.1 0.38 0.2 0.4 0.3 0.42 0.42 0.44 Plastic Strain Ratio : 1.88 Initial Strain : 0.02mm/mm Hardening Exponent : 0.22 Strength Coefficient : 686.7662MPa

======== Thermal/Electrical Thermal Expansion Coefficient (A) : 1.728e-05C Thermal Conductivity (K) : 14000W/(mmC) Specific Heat (CP) : 434000000J/(kgK)

======== Creep : 0

======== Viscoelasticity Model : 0

======== Viscoplasticity Viscoplastic Type : 0

======== Damage : 3

======== Miscellaneous Fixed Stock Thickness : 0 Adhesive : Not Defined Adult HIC1000 Offset : 95mm Adult HIC1700 Offset : 74mm Child HIC1000 Offset : 85mm Child HIC1700 Offset : 68mm Leg Impact Offset : 50mm NCAP Adult 650 Offset : 115mm NCAP Child 650 Offset : 105mm NCAP Adult 1000 Offset : 94mm NCAP Child

1000 Offset : 90mm NCAP Adult 1350 Offset : 74mm NCAP Child 1350 Offset : 70mm NCAP Adult 1700 Offset : 65mm NCAP Child 1700 Offset : 60mm Crosshatch Pattern : Steel

---

MATERIAL INFORMATION

Material : Falicon ASTM A304

Parent Material : Falicon ASTM A304 Parent Material Location : CRF250L-Falicon-Rod1

Material properties: Locally defined material Material Type: Isotropic Label: 1 Alternate Name : Category : METAL Sub-Category : Alloy Steel Mass Density (RHO) : 7700 kg/m

======== Mechanical Young's Modulus (E) : 210000 MPa : Major Poisson's Ratio Poisson's Ratio (NU) : 0.3 Shear Modulus (G) : Not defined Structural Damping Coefficient (GE) : Not defined Stress-Strain Input Data Type : Engineering Stress-Strain Stress-Strain (H) : Stress-Strain (H)(1) Type of Nonlinearity (TYPE) : PLASTIC Yield Function Criterion (YF) : von Mises Hardening Rule (HR) : Isotropic Initial Yield Point (LIMIT1) : 235000 kPa Initial Friction Angle (LIMIT2) : Not defined Mechanical Power to Heat Ratio : 0

======== Strength Yield Strength : 2500 MPa Ultimate Tensile Strength : 2600 MPa Tsai-Wu Interaction Coefficient (F12): Not defined Tension (ST) : Not defined Compression (SC) : Not defined Shear (SS) : Not defined Tension (XT) : Not defined Compression (XC) : Not defined Shear (XS) : Not defined

======== Durability Stress-Life Data : Expression Fatigue Strength Coefficient : Not defined Fatigue Strength Exponent : Not defined Strain-Life Data : Expression Fatigue Ductility Coefficient : Not defined Fatigue Ductility Exponent : Not defined Cyclic Yield Strength : Not defined Cyclic Strength Coefficient : Not defined Cyclic Strain Hardening Exponent : Not defined Fatigue Limit Strength in Bending : Not defined Fatigue Limit Strength in Torsion : Not defined Percent Reduction in Area : 0 R-Ratio : Specify : -1 Test Type : Tension Survival Probability : 50 Tsigma (90/10) : 1.5 : Cycles Number of Cycles : Not defined

======== Formability Work Hardening : 0.22 Forming Limit : Forming Limit(1) Plastic Strain Ratio : 1.88 Initial Strain : 0.02 mm/mm Hardening Exponent : 0.22 Strength Coefficient : 686.7662 MPa R0 : 2.3 R45 : 2.8 R90 : 3.1 Bend Radii - SI Material Stock : No Field Bend Radii - English Material Stock : No Field

======== Thermal/Electrical Temperature (TREF) : Not defined Thermal Expansion Coefficient (A) : 1.728e-05 C Thermal Conductivity (K) : 14000 W/(mmC) Specific Heat (CP) : 434000000 J/(kgK) Latent Heat (L) : Not defined Phase Change Temperature : Not defined Phase Change Temperature Range : Not defined Specific Heat Above Phase Change : Not defined Resistivity : Not defined Scattering : Not defined Extinction : Not defined Scattering : Not defined Extinction : Not defined

======== Creep : None

======== Viscoelasticity Model : None

======== Viscoplasticity Viscoplastic Type : None

======== Damage : None

======== Miscellaneous Fixed Stock Thickness : false Default Thickness : Not defined Adhesive : Adult HIC1000 Offset : Not defined Adult HIC1700 Offset : Not defined Child HIC1000 Offset : Not defined Child HIC1700 Offset : Not defined Leg Impact Offset : Not defined NCAP Adult 650 Offset : Not defined NCAP Child 650 Offset : Not defined NCAP Adult 1000 Offset : Not defined NCAP Child 1000 Offset : Not defined NCAP Adult 1350 Offset : Not defined NCAP Child 1350 Offset : Not defined NCAP Adult 1700 Offset : Not defined NCAP Child 1700 Offset : Not defined Crosshatch Pattern : Steel

======== Stress-Strain (H)(1) 0 0 0.00114 235000 0.0296 237000 0.0392 255000 0.0488 270000 0.0583 283000 0.0677 295000 0.077 306000 0.0862 315000 0.0953 323500 0.1044 331500 0.1133 338500 0.1222 343500 0.131 348000 0.1484 356500 0.157 360500 0.1655 364200 0.174 367500 0.1823 370500 0.2 376700 0.3 406000 0.4 430000 0.5 450000 0.6 468000 0.7 483000 0.8 496000 0.9 508000 1 520000

======== Forming Limit(1) -0.5 0.88 0.02 0.35 0.1 0.38 0.2 0.4 0.3 0.42 0.42 0.44

MATERIAL INFORMATION

Material : Bearing material

Material properties: Referenced library material : Bearing-material.xml Library Version : 1.0 Material Type: Isotropic Label: 1 Alternate Name : Category : METAL Sub-Category : Alloy Steel Mass Density (RHO) : 1 kg/m

======== Mechanical Young's Modulus (E) : 113000000 kPa : Major Poisson's Ratio Poisson's Ratio (NU) : 0.3 Shear Modulus (G) : Not defined Structural Damping Coefficient (GE) : Not defined Stress-Strain Input Data Type : Undefined Stress-Strain (H) : Stress-Strain (H) Type of Nonlinearity (TYPE) : PLASTIC Yield Function Criterion (YF) : von Mises Hardening Rule (HR) : Isotropic Initial Yield Point (LIMIT1) : 235000 kPa Initial Friction Angle (LIMIT2) : Not defined Mechanical Power to Heat Ratio : 0

======== Strength Yield Strength : 1825000 kPa Ultimate Tensile Strength : 2320000 kPa Tsai-Wu Interaction Coefficient (F12): Not defined Tension (ST) : Not defined Compression (SC) : Not defined Shear (SS) : Not defined Tension (XT) : Not defined Compression (XC) : Not defined Shear (XS) : Not defined

======== Durability Stress-Life Data : Expression Fatigue Strength Coefficient : Not defined Fatigue Strength Exponent : Not defined Strain-Life Data : Expression Fatigue Ductility Coefficient : Not defined Fatigue Ductility Exponent : Not defined Cyclic Yield Strength : Not defined Cyclic Strength Coefficient : Not defined Cyclic Strain Hardening Exponent : Not defined Fatigue Limit Strength in Bending : Not defined Fatigue Limit Strength in Torsion : Not defined Percent Reduction in Area : 0 R-Ratio : Specify : -1 Test Type : Tension Survival Probability : 50 Tsigma (90/10) : 1.5 : Cycles Number of Cycles : Not defined

======== Formability Work Hardening : 0.22 Forming Limit : Forming Limit Plastic Strain Ratio : 1.88 Initial Strain : 0.02 mm/mm Hardening Exponent : 0.22 Strength Coefficient : 686.7662 MPa R0 : 2.3 R45 : 2.8 R90 : 3.1 Bend Radii - SI Material Stock : No Field Bend Radii - English Material Stock : No Field

======== Thermal/Electrical Temperature (TREF) : Not defined Thermal Expansion Coefficient (A) : 1.728e-05 C Thermal Conductivity (K) : 14000 W/(mmC) Specific Heat

(CP) : 434000000 J/(kgK) Latent Heat (L) : Not defined Phase Change Temperature : Not defined Phase Change Temperature Range : Not defined Specific Heat Above Phase Change : Not defined Resistivity : Not defined Scattering : Not defined Extinction : Not defined Scattering : Not defined Extinction : Not defined

======== Creep : None

======== Viscoelasticity Model : None

======== Viscoplasticity Viscoplastic Type : None

======== Damage : None

======== Miscellaneous Fixed Stock Thickness : false Default Thickness : Not defined Adhesive : Adult HIC1000 Offset : 95 mm Adult HIC1700 Offset : 74 mm Child HIC1000 Offset : 85 mm Child HIC1700 Offset : 68 mm Leg Impact Offset : 50 mm NCAP Adult 650 Offset : 115 mm NCAP Child 650 Offset : 105 mm NCAP Adult 1000 Offset : 94 mm NCAP Child 1000 Offset : 90 mm NCAP Adult 1350 Offset : 74 mm NCAP Child 1350 Offset : 70 mm NCAP Adult 1700 Offset : 65 mm NCAP Child 1700 Offset : 60 mm Crosshatch Pattern : Steel

======== Stress-Strain (H) 0 0 0.00114 235000 0.0296 237000 0.0392 255000 0.0488 270000 0.0583 283000 0.0677 295000 0.077 306000 0.0862 315000 0.0953 323500 0.1044 331500 0.1133 338500 0.1222 343500 0.131 348000 0.1484 356500 0.157 360500 0.1655 364200 0.174 367500 0.1823 370500 0.2 376700 0.3 406000 0.4 430000 0.5 450000 0.6 468000 0.7 483000 0.8 496000 0.9 508000 1 520000

======== Forming Limit -0.5 0.88 0.02 0.35 0.1 0.38 0.2 0.4 0.3 0.42 0.42 0.44

MATERIAL INFORMATION

Material : Steel-Rolled-1

Parent Material : Steel-Rolled Parent Material Library : physicalmateriallibrary.xml Parent Material Library Version : 4.0

Material properties: Locally defined material Material Type: Isotropic Label: 2 Alternate Name : Category : METAL Sub-Category : Alloy Steel Mass Density (RHO) : 7657 kg/m

======== Mechanical Young's Modulus (E) : 206000000 kPa : Major Poisson's Ratio Poisson's Ratio (NU) : 0.3 Shear Modulus (G) : Not defined Structural Damping Coefficient (GE) : Not defined Stress-Strain Input Data Type : Engineering Stress-Strain Stress-Strain (H) : Stress-Strain (H) Type of Nonlinearity (TYPE) : PLASTIC Yield Function Criterion (YF) : von Mises Hardening Rule (HR) : Isotropic Initial Yield Point (LIMIT1) : 235000 kPa Initial Friction Angle (LIMIT2) : Not defined Mechanical Power to Heat Ratio : 0

======== Strength Yield Strength : 235000 kPa Ultimate Tensile Strength : 340000 kPa Tsai-Wu Interaction Coefficient (F12): Not defined Tension (ST) : Not defined Compression (SC) : Not defined Shear (SS) : Not defined Tension (XT) : Not defined Compression (XC) : Not defined Shear (XS) : Not defined

======== Durability Stress-Life Data : Expression Fatigue Strength Coefficient : Not defined Fatigue Strength Exponent : Not defined Strain-Life Data : Expression Fatigue Ductility Coefficient : Not defined Fatigue Ductility Exponent : Not defined Cyclic Yield Strength : Not defined Cyclic Strength Coefficient : Not defined Cyclic Strain Hardening

Exponent : Not defined Fatigue Limit Strength in Bending : Not defined Fatigue Limit Strength in Torsion : Not defined Percent Reduction in Area : 0 R-Ratio : Specify : -1 Test Type : Tension Survival Probability : 50 Tsigma (90/10) : 1.5 : Cycles Number of Cycles : Not defined

======== Formability Work Hardening : 0.22 Forming Limit : Forming Limit Plastic Strain Ratio : 1.88 Initial Strain : 0.02 mm/mm Hardening Exponent : 0.22 Strength Coefficient : 686.7662 MPa R0 : 2.3 R45 : 2.8 R90 : 3.1 Bend Radii - SI Material Stock : No Field Bend Radii - English Material Stock : No Field

======== Thermal/Electrical Temperature (TREF) : Not defined Thermal Expansion Coefficient (A) : 1.728e-05 C Thermal Conductivity (K) : 14000 W/(mmC) Specific Heat (CP) : 434000000 J/(kgK) Latent Heat (L) : Not defined Phase Change Temperature : Not defined Phase Change Temperature Range : Not defined Specific Heat Above Phase Change : Not defined Resistivity : Not defined Scattering : Not defined Extinction : Not defined Scattering : Not defined Extinction : Not defined

======== Creep : None

======== Viscoelasticity Model : None

======== Viscoplasticity Viscoplastic Type : None

======== Damage : None

======== Miscellaneous Fixed Stock Thickness : false Default Thickness : Not defined Adhesive : Adult HIC1000 Offset : Not defined Adult HIC1700 Offset : Not defined Child HIC1000 Offset : Not defined Child HIC1700 Offset : Not defined Leg Impact Offset : Not defined NCAP Adult 650 Offset : Not defined NCAP Child 650 Offset : Not defined NCAP Adult 1000 Offset : Not defined NCAP Child 1000 Offset : Not defined NCAP Adult 1350 Offset : Not defined NCAP Child 1350 Offset : Not defined NCAP Adult 1700 Offset : Not defined NCAP Child 1700 Offset : Not defined Crosshatch Pattern : Steel

======== Stress-Strain (H) 0 0 0.00114 235000 0.0296 237000 0.0392 255000 0.0488 270000 0.0583 283000 0.0677 295000 0.077 306000 0.0862 315000 0.0953 323500 0.1044 331500 0.1133 338500 0.1222 343500 0.131 348000 0.1484 356500 0.157 360500 0.1655 364200 0.174 367500 0.1823 370500 0.2 376700 0.3 406000 0.4 430000 0.5 450000 0.6 468000 0.7 483000 0.8 496000 0.9 508000 1 520000

======== Forming Limit -0.5 0.88 0.02 0.35 0.1 0.38 0.2 0.4 0.3 0.42 0.42 0.44

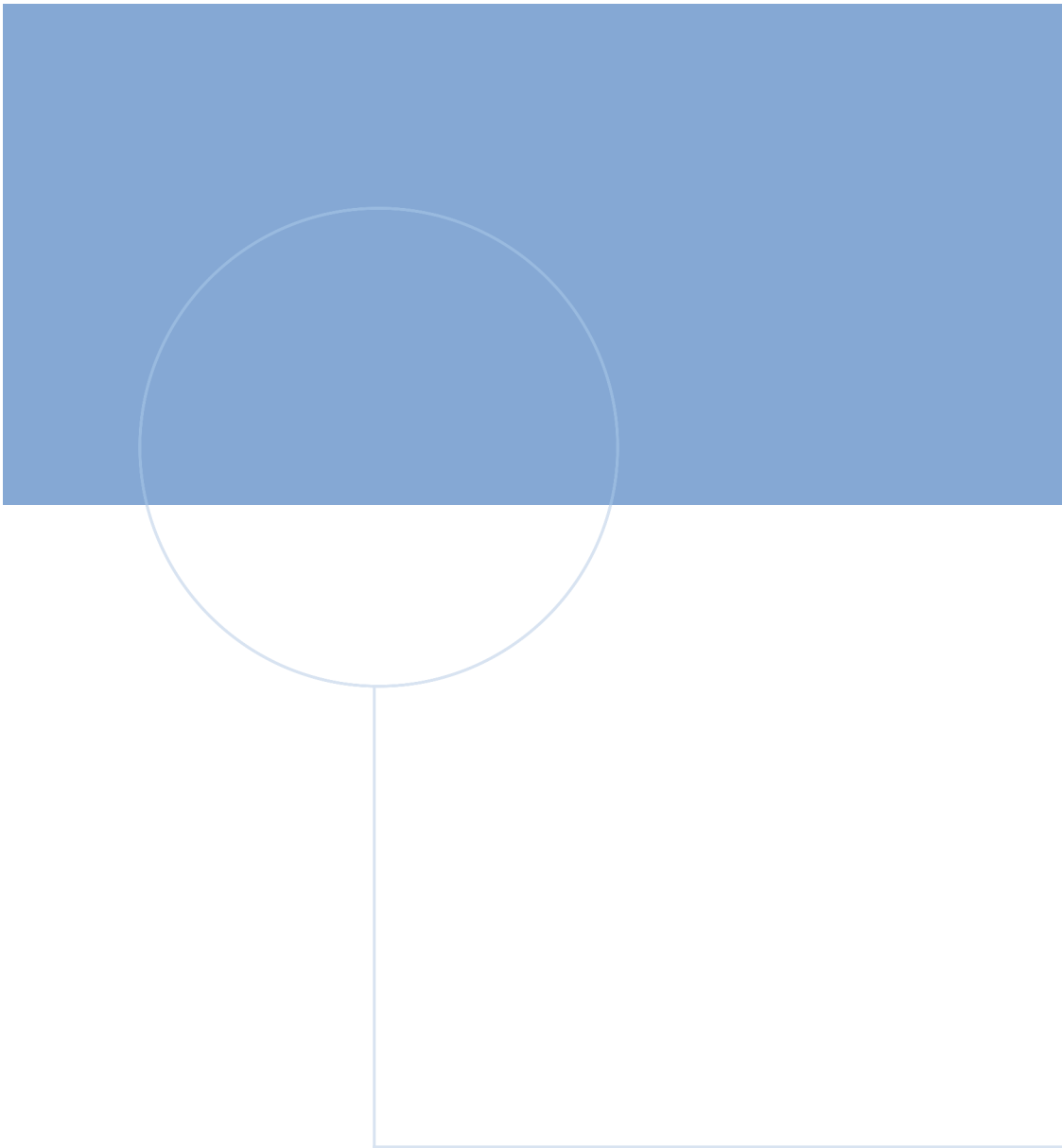

NTNU

Kunnskap for en bedre verden